

Chapter 7

An introduction to dynamical systems

All living things and their component cells are dynamical systems. The molecules that form us are constantly in flux, changing in location and number throughout our bodies; cells, including neurons, are generated and die; connections between neurons form and disappear; activity in neural circuits rises and falls. Yet, beneath the fluidity and apparent tumult within the processes that comprise a living being, is a choreography that ensures stability of the key patterns that make us who we are. To gain a better understanding of this choreography we should first embrace the mathematical framework of dynamical systems. In this chapter, we summarize the properties and roles of dynamical systems used within this book, many of which we have discussed in earlier chapters.

For a more in-depth study of the role of dynamical systems in neuroscience, in particular at the single-neuron level, I highly recommend the book, *Dynamical Systems in Neuroscience* by Eugene Izhikevich¹. For a more pedagogical approach to the mathematics of dynamical systems in general, *Nonlinear Dynamics and Chaos* by Steven Strogatz² is exceptionally good.

7.1. What is a dynamical system?

In simplest terms a dynamical system is one in which the variables can change in time, *i. e.*, are dynamic. Mathematically the term is typically reserved for the study of systems of nonlinear differential equations—such as those we have been using to describe neural activity.

As we have seen, a differential equation is needed to describe just about any biophysical process—rates of change of concentrations of molecules depend on concentrations of other molecules; rate of entry of ions into a cell depends on the fraction of open ion channels; rate of ion channel opening depends on the membrane potential, or temperature, or neurotransmitter release; rate of population growth of a species depends on numbers of that species, predators, and available food stocks. All of these processes are described via the rates of change of the corresponding variables. Moreover, the dependencies are nonlinear—thresholds, saturation, power-law and exponential dependences abound—except in very simple cases rarely seen in biology. Thus, nonlinear differential equations comprise the correct approach to modeling—and perhaps a key to the understanding (*e. g.*,³)—neural activity and, indeed, any biological system.

In the following sections, we explore the various behaviors of dynamical systems, predominantly using as a basis the firing rate model of neural activity (Chapter 6). We shall see that even simple circuits can exhibit multiple, qualitatively distinct types of behavior, just as the membrane potential of a bistable neuron can oscillate or remain static. Moreover, quantitative changes in the values of parameters of a given circuit can produce dramatic, qualitative transitions in the circuit's behavior. The study of such transitions is the hallmark of courses in dynamical systems, whose key message applies to all biological systems: a significant change in behavior can be caused by a subtle, barely observable change in the system's parameters.

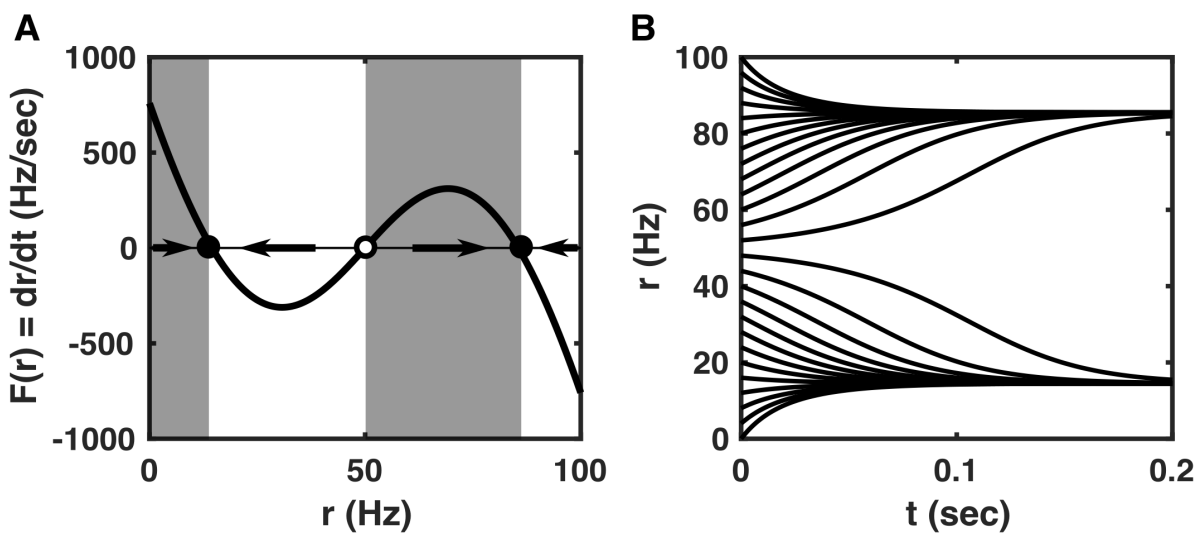


Figure 7.1. Stable and unstable fixed points in a single-variable firing rate model.

A) A plot of $\frac{dr}{dt}$ against r , where $\frac{dr}{dt} = F(r) = \frac{-r+100/\{1+\exp[-(Wr-I_{th})/I_\sigma]\}}{\tau}$ is obtained from a firing-rate model with recurrent feedback of strength W (see Section 6.3). In this example, there are three fixed points (denoted by circles where $F(r) = 0$). Fixed points separate ranges of r where $\frac{dr}{dt} > 0$ (shaded gray) from ranges where $\frac{dr}{dt} < 0$ (unshaded). Arrows on the x-axis indicate the direction of change of r (rightward to increase r where $\frac{dr}{dt} > 0$ and leftward to decrease r where $\frac{dr}{dt} < 0$). The solid circles are stable fixed points, around which the direction of $\frac{dr}{dt}$ is toward the fixed point, while the open circle at 50Hz is an unstable fixed point, around which the direction of $\frac{dr}{dt}$ is away from the fixed point. The system is bistable and can be a basic memory unit. **B)** If the differential equation is simulated with multiple starting points, the trajectories of $r(t)$ move away from the unstable fixed point and toward one of the stable fixed points. Notice that since $\frac{dr}{dt}$ depends only on r , if one were to take any horizontal line of fixed r , the gradient of the trajectories crossing that line would all be the same (fixed $\frac{dr}{dt}$ at a fixed r). Parameters used are $\tau = 10\text{ms}$, $W = 1\text{nA/Hz}$, $I_{th} = 50\text{nA}$, $I_\sigma = 20\text{nA}$. This figure was generated by the online code `drdt_plot.m`.

7.2. Single variable behavior and fixed points

Box 7.1. Fixed point: A set of values of all variables of a system at which none of the variables change in time (the right-hand side of all ODEs evaluates to zero).

For a single variable, such as firing rate, r , the dynamical system can be expressed as:

$$\frac{dr}{dt} = F(r), \quad \text{Eq. 7.1}$$

where $F(r)$ can be any, generally nonlinear, function. While we know how to solve such an equation computationally, its qualitative behavior can be understood simply by plotting

$F(r)$ as a function of r . As we have seen, any value of r at which $F(r) = 0$ is a fixed point, since when set at that value, r does not change. Of importance is whether, if shifted slightly away from the fixed point, r moves further away or returns toward the fixed point. The former case corresponds to an unstable fixed point, the latter case corresponds to a stable fixed point. Stable fixed points are important as they correspond to stable states or equilibria, to which activity is drawn. These are usually dynamic equilibria at which the ongoing processes conspire to ensure the rate of increase of any variable is precisely countered by its rate of decrease. Unstable fixed points correspond to tipping points, or points of no return. The value of $F(r)$ either side of the fixed point tells us the direction in which r moves, so tells us the fixed point's stability (Figure 7.1).

7.2.1. Bifurcations

Box 7.2. Bifurcation: A bifurcation occurs when a continuous change in a parameter at some point leads to a qualitative change in the behavior of a system, usually because the number and/or stability of fixed points changes at that value of the parameter.

Figure 7.1 was generated from a firing-rate model with fixed values for the feedback strength, W , and the firing threshold, I_{th} (see Chapter 6). When either of these parameters are altered, the position of the fixed points changes and even the numbers of fixed points can change. In particular, if the feedback is too weak or the threshold is too high, then the state of high firing rate is no longer present. Conversely, if the feedback is too strong or the threshold is too low, then the state of low firing rate disappears.

For example, if we increase the value of excitatory feedback, W , from that of Figure 7.1A (as would happen if synaptic strengths were increased), $\frac{dr}{dt}$ would increase, shifting the curve up. As the curve of $\frac{dr}{dt}$ versus r rises with such an increase of W , we see that the lower stable fixed point and the unstable fixed point approach each other (Figure 7.2A-B) until they collide at a critical value of W (Figure 7.2C). If W is further increased then only a high firing-rate stable fixed point remains (Figure 7.2D). Conversely, if we were to decrease

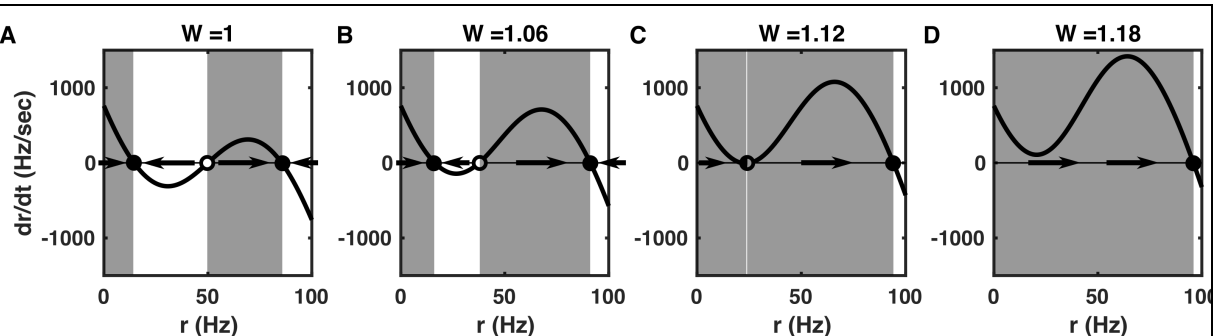


Figure 7.2. Increase of feedback strength causes loss of low firing-rate fixed point.

A. The bistable system of Figure 7.1. B. With increased feedback, W , dr/dt becomes more positive, so the curve shifts up and the lower fixed points move closer together. C. At a critical value of feedback the lower two fixed points collide. D. With even greater feedback, only one fixed point remains. These curves were produced using the online code `drdt_plot_manyW.m`.

the value of W then the higher stable fixed point and the unstable one would approach each other until they collide. If W were decreased further then only a low firing-rate stable fixed point would remain.

We can combine these results into one figure to show how the fixed points change as we vary the feedback parameter, W . The resulting figure is a bifurcation plot (Figure 7.3), in which the firing-rates given by the x-coordinates of the intercepts (the circles) in Figure 7.2 are now plotted on the y-axis. As the parameter, W , is gradually varied along the x-axis, points arise where there is an abrupt change in the number or the stability of fixed points—these are the points of bifurcation.

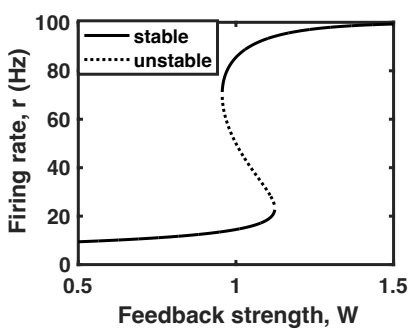


Figure 7.3. A bifurcation curve shows the stable and unstable states as a function of a control parameter. The feedback strength, W , controls whether the system has a single stable state of low firing rate (at low W), a single stable state of high firing rate (at high W), or two stable states with an intermediate unstable fixed point (at intermediate W). Two bifurcations occur with increasing W , one at the appearance, the other at the disappearance of the unstable fixed point. The x-axis crossing-points of the curves in Figure 7.2 produce points on this curve: three points at feedback strengths of $W = 1$ and $W = 1.06$ (Figure 7.2A and B); one point of high rate at $W = 1.18$ (Figure 7.2D), with $W = 1.12$ (Figure 7.2C) corresponding to the bifurcation point, at the value of W where the two lower fixed points collide. This figure was generated by the online code `bifurcation_varyW.m`.

7.2.2. Requirement for oscillations

Single variable dynamics of the form of Eq. 7.1, are quite constrained in their behaviors. For example, oscillations are not possible, because an oscillation requires the variable to change back and forth, so that at any value in its oscillating range, the variable's rate of change should be positive when on the increasing part of the cycle, but negative when on the decreasing part of the cycle. Such behavior is incompatible with Eq. 7.1, which provides a single value for the rate of change at each value of the variable, r .

However, we saw in Chapter 2 that periodic activity is possible in a single-variable model such as the leaky integrate-and-fire model, if there is a mapping that instantaneously changes the value of the variable from one value to another. In these simple models of the neuron's membrane potential, the reset, by means of which the membrane potential instantaneously jumps from the high value (the threshold, V_{th}) to a lower value (the reset potential, V_{reset}) is essential to allow regular spiking. Such a mapping is akin to taking a sheet of paper with an x-axis drawn on it, then rolling it into a cylinder such that the highest x-value connects to the lowest x-value. Using a pencil to draw a line, if one is only allowed to extend the line in a single direction, (*e.g.* if x only increases with time) the line

will keep returning to itself periodically, so its x-coordinate will oscillate. Without such a mapping, two variables are needed to produce an oscillator.

7.3. Models with two variables

A rich variety of behaviors—including many important ones observed in real neurons and circuits—are possible in models of dynamical systems that possess two variables. The behavior of two variables can be plotted in two dimensions (one axis for each variable) so can be easily visualized. Because of these two features, it is very common for mathematicians to try to reduce more complicated models to two-variable ones.

For example, the Hodgkin-Huxley model (Eq. 4.9) can be reduced from four variables (V, m, h, n) to two variables (V, w). First, the need for a separate dynamical equation for the activation variable, m , is removed by assuming that it changes instantaneously with membrane potential, V . Second, sodium inactivation, h , and potassium activation, n , respond to changes in membrane potential with similar time constants, so that the value of one of them is highly predictive of the value of the other. Therefore, they can be combined into a single variable, w . The FitzHugh-Nagumo model⁴⁻⁶, which we shall study in Section 7.6, is a simplified version of this two-variable reduction.

In general, a two-variable model requires two differential equations, each of which can depend on both variables. For example, with two connected firing-rate units, the general form is:

$$\begin{aligned}\frac{dr_1}{dt} &= F(r_1, r_2) \\ \frac{dr_2}{dt} &= G(r_1, r_2)\end{aligned}\quad \text{Eq. 7.2}$$

where $F(r_1, r_2)$ and $G(r_1, r_2)$ are typically two different functions, either because the two units represent different cell-types, or because the connections they receive are not identical. For example, in the decision-making circuit of Section 6.5, where

$$\begin{aligned}\tau \frac{dr_1}{dt} &= -r_1 + f(W_s r_1 + W_x r_2) \\ \tau \frac{dr_2}{dt} &= -r_2 + f(W_s r_2 + W_x r_1)\end{aligned}\quad \text{Eq. 7.3}$$

and $f(I)$ is the single-neuron firing-rate response to input current, I , the two functions are $F(r_1, r_2) = [-r_1 + f(W_s r_1 + W_x r_2)]/\tau$ and $G(r_1, r_2) = [-r_2 + f(W_s r_2 + W_x r_1)]/\tau$.

Just as in single-variable models, the location and type of fixed points are key determinants of the behavior of a two-variable model. To see the fixed points and understand how they change with changes in parameters, it is useful to plot nullclines using phase-plane analysis, as will be explained in the next subsection.

Box 7.3. Nullcline: A curve showing how the fixed point of one variable depends on the values of other variables in a system of coupled ODEs.

Box 7.4. Phase plane: A plot on the axes of the two variables in a system of two coupled ODEs, which can show the position of fixed points, nullclines, and trajectories demonstrating how the variable of the system change together over time.

7.3.1 Nullclines and phase-plane analysis

At a fixed point of a two-variable system, it is necessary that both differential equations produce zero rate of change, *i.e.*, $F(r_1, r_2) = 0$ and $G(r_1, r_2) = 0$ in Eq. 7.2. To produce nullclines, we consider one of these equations at a time. By way of example we will consider a decision-making circuit with threshold-linear units, in the absence of a stimulus:

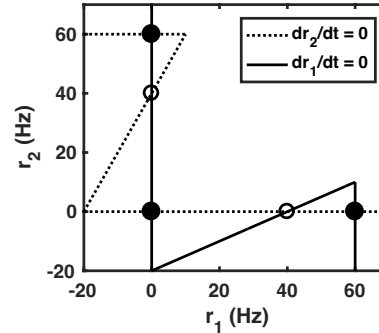
$$\begin{aligned}\tau \frac{dr_1}{dt} &= -r_1 + W_s r_1 + W_x r_2 - \Theta \\ \tau \frac{dr_2}{dt} &= -r_2 + W_s r_2 + W_x r_1 - \Theta,\end{aligned}\quad \text{Eq. 7.4}$$

where $\Theta > 0$ is the threshold, proportional to the amount of input current the neurons need to start firing spikes (as in Tutorial 6.2). A negative threshold ($\Theta < 0$) corresponds to a rate of spontaneous activity, the firing rate in the absence of input.

Considering the second of Eq. 7.4, we find that $\frac{dr_2}{dt} = 0$ if

$$r_2 = \frac{W_x r_1 - \Theta}{1 - W_s}, \quad \text{Eq. 7.5}$$

Figure 7.4. Nullclines showing the fixed points of a bistable system with threshold-linear firing-rate units. The nullcline for r_2 is shown as a dotted line, and for r_1 as a solid line. The nullclines cross at 5 fixed points, 3 of which are stable (solid circles) and 2 of which are unstable (open circles). The axes are extended to negative rates—which can never be reached in practice—so that the complete “Z” shape of the nullclines can be seen. The shapes of the curves are similar to reflections of Figure 7.3 (reflected, because rate of one unit provides negative input to the other). In this case, the fixed points all lie on one of the axes. The online code “nullcline_bistable.m” was used to generate this figure. It can be altered so that the parameter-dependence of the nullclines and fixed points is easily studied.



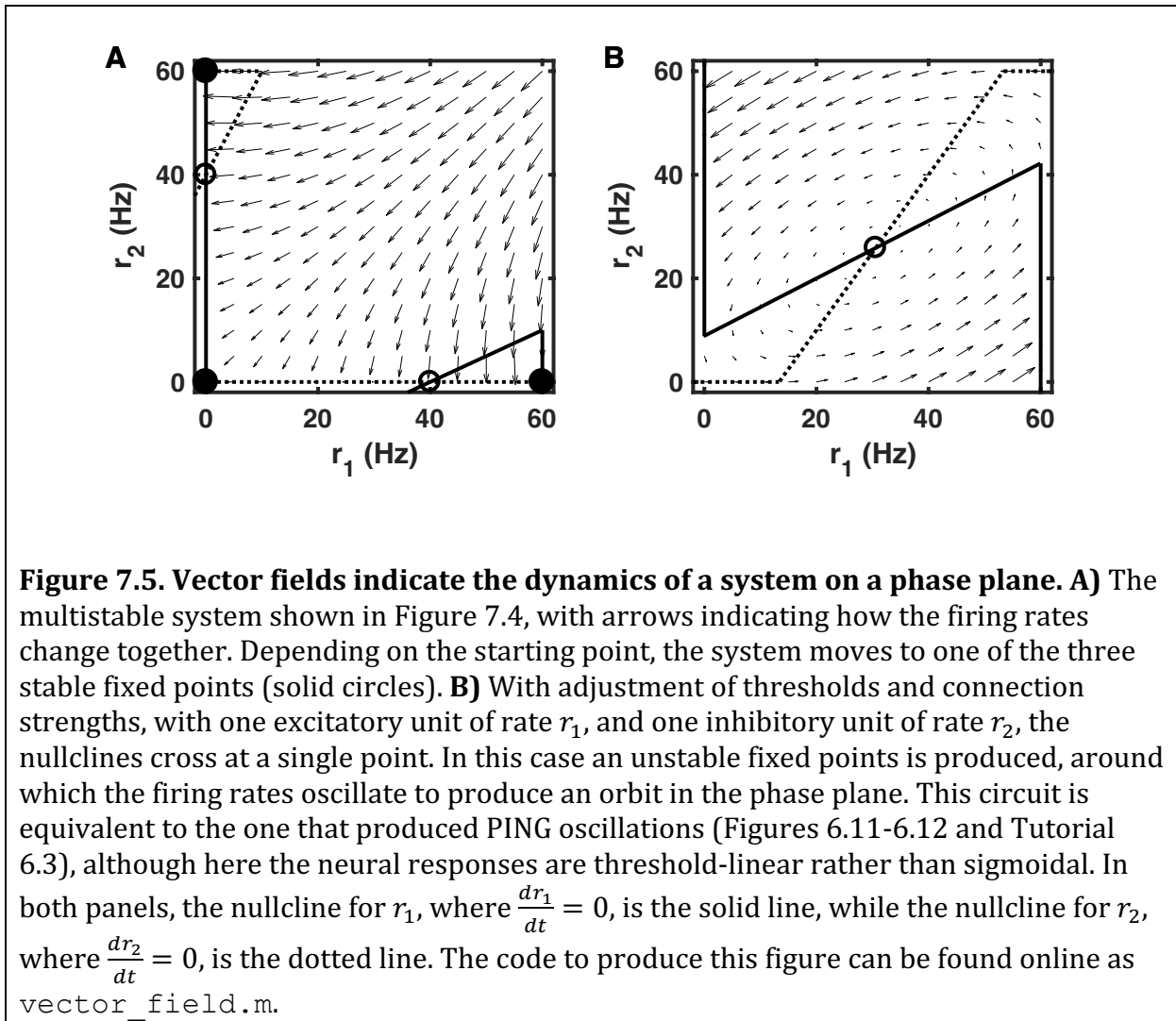
which describes a straight line if we plot r_2 against r_1 . This straight line forms one of the two nullclines of the system. It shows the values of r_2 where $\frac{dr_2}{dt} = 0$ (*i.e.*, fixed points of r_2) if r_1 were held constant.

We also can show that if firing rates are constrained to be nonnegative then $\frac{dr_2}{dt} = 0$ if $r_2 = 0$ and $W_x r_1 - \Theta < 0$, since $\frac{dr_2}{dt}$ is prevented from being negative in this situation. Similarly, if there is a maximum firing rate of r_{max} , then $\frac{dr_2}{dt} = 0$ if $r_2 = r_{max}$ and $-r_{max} + W_s r_{max} + W_x r_1 - \Theta > 0$, since $\frac{dr_2}{dt}$ is prevented from being positive in this situation.

For concreteness, to find these fixed points, we will use the parameters of Tutorial 6.2 (jumping mode): $r_{max} = 60\text{Hz}$, $W_s = 1.05$, $W_x = -0.05$, and $\Theta = 4\text{Hz}$. In this case, the dotted line of Figure 7.4 is the resulting nullcline for r_2 . Notice it has three parts, one

following Eq. 7.5 in a diagonal direction, one horizontal at $r_2 = 0$ where the dynamics alone would reduce r_2 further, and one horizontal at $r_2 = r_{max}$, where the dynamics alone would increase r_2 further.

Similarly, by solving for how r_1 varies with r_2 when $\frac{dr_1}{dt} = 0$ in Eq. 7.4, we obtain a second nullcline, the solid curve in Figure 7.4, whose diagonal portion follows the equation:



$$r_1 = \frac{W_x r_2 - \Theta}{1 - W_s}. \quad \text{Eq. 7.6}$$

We then know that at the points where these two curves cross, both $\frac{dr_1}{dt} = 0$ and $\frac{dr_2}{dt} = 0$, so the system has a fixed point—a pair of values of (r_1, r_2) such that if the system were set at these rates, the rates would not change.

We can rearrange Eq. 7.6 to obtain $r_2 = \frac{(1-W_s)r_1 + \Theta}{W_x}$. Then we can see that Eq. 7.6 produces the same line as Eq. 7.5 if the gradients are the same, such that $(1 - W_s)/W_x =$

$W_x/(1 - W_s)$, and if the intercepts are the same, such that $\Theta/W_x = -\Theta/(1 - W_s)$. Therefore, if we set $W_x = -(1 - W_s)$ or $W_s - W_x = 1$, then the two lines are identical and the nullclines overlap along a straight line. This is identical to the requirement for an integrator in a decision-making circuit (see text following Eq. 6.14) and we used this condition for one circuit in Tutorial 7.2.

In addition to the nullclines, it can also be useful to plot arrows indicating the direction of change of firing rates (Figure 7.5). Unlike the single-variable case depicted in Figure 7.1, the arrows do not demonstrate with certainty whether a fixed point is stable, but they do provide a good indication. They can also suggest when oscillations occur, as oscillations appear as orbits around a fixed point when plotted as a function of two variables on a plane (Figure 7.5B).

Box 7.5. Orbit: A closed trajectory, showing how the variables of the system can change together over time such that they return to their starting state, implying an oscillation of the system.

7.3.2. The inhibition-stabilized network

Before looking at time-varying dynamical states, we consider here a stable fixed point that has unexpected, sometimes considered paradoxical properties in its response to external input⁷. Given the strength of feedback excitation and inhibition in many areas of the brain, and careful modeling of the observed neural activity patterns in both visual cortex and hippocampus, there is reason to believe some neural circuits operate in an inhibition-stabilized regime⁸.

Box 7.6. Inhibition-stabilized regime: The set of parameters in which a circuit has sufficient excitatory feedback to destabilize any low firing-rate state, but with sufficient compensatory inhibitory feedback to stabilize the excitatory rate at a value that, without dynamic inhibitory feedback, would be an unstable fixed point intermediate between its low spontaneous rate and its high, saturated rate.

To be in the inhibition-stabilized regime (Figure 7.6), one requirement is that the excitatory feedback to excitatory neurons (W^{EE} in Figure 7.6A-B) is sufficiently strong that, in the absence of inhibition, the excitatory cells would not be able to fire stably at a low rate—the feedback is so strong that each spike generates more than one extra spike, so the spike rate would increase until a maximum rate (or maximum level of feedback) is reached (as we saw in Figure 7.2D).

The second requirement for a circuit to be in the inhibition-stabilized regime is that the inhibitory unit's nullcline (the dotted line of Figures 7.6C-D) crosses the excitatory unit's nullcline on its unstable branch. To see this, consider the fixed point (the solid circle) on Figure 7.6C. We see that if we move to the left then the arrows point leftward because $\frac{dr_1}{dt} < 0$, while if we move to the right then the arrows point rightward because $\frac{dr_1}{dt} > 0$. That is, considering only the x-direction the arrows point away from the diagonal solid line and toward the vertical solid lines at $r_1 = 0$ and at $r_1 = 60\text{Hz}$. That is, if we do not take into

account changes in inhibition, so fix r_2 , the dynamics of r_1 alone corresponds to the situation in Figure 7.1, with an intermediate, unstable fixed point.

The third and final requirement for the circuit to be in the inhibition stabilized regime is that the inhibitory feedback is sufficient to stabilize the fixed point in question.

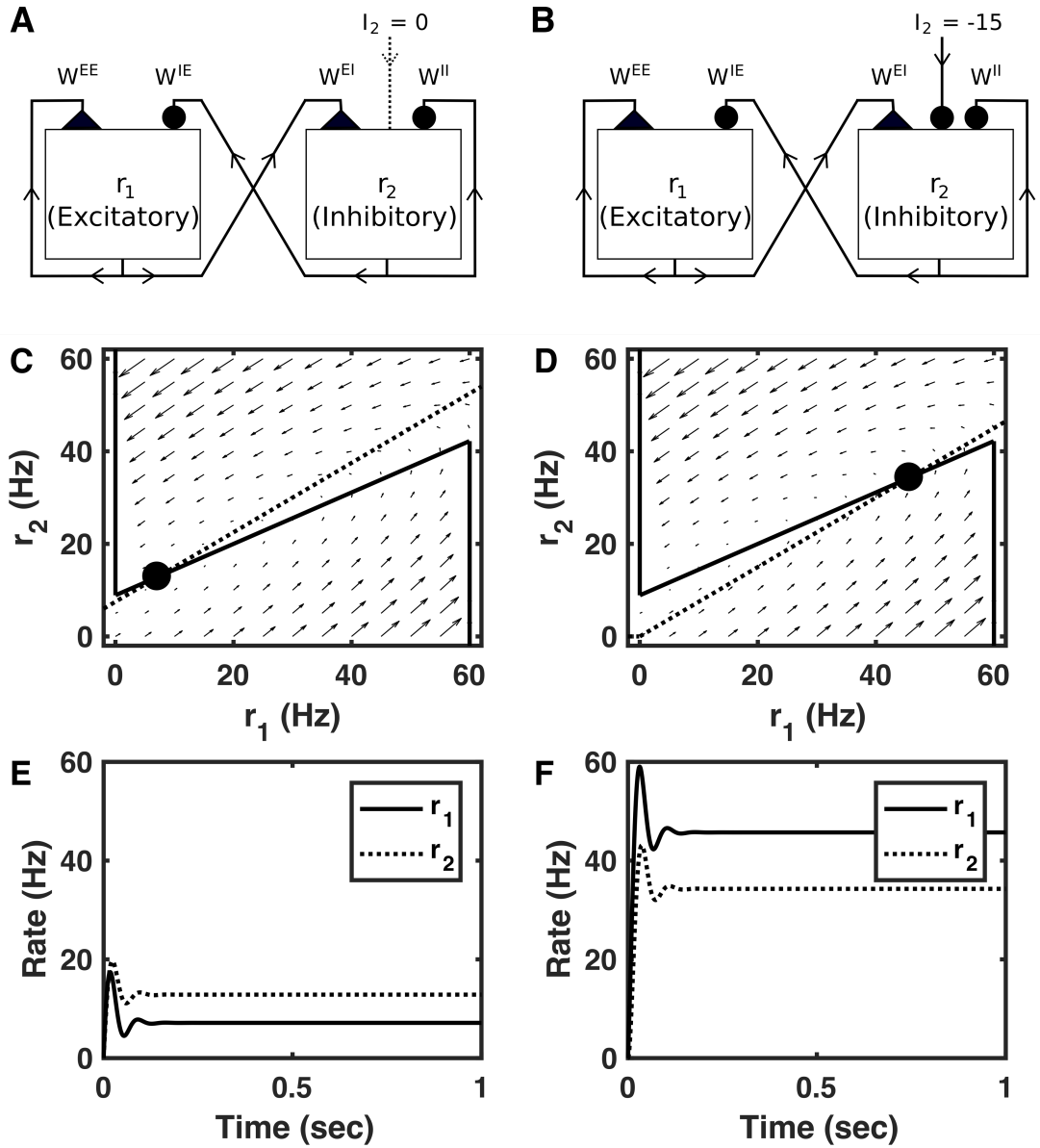


Figure 7.6. The surprising response to inputs of an inhibition-stabilized network.

A-B. The circuit consists of two units, one excitatory and one inhibitory, with strong excitatory (solid triangles) and inhibitory (solid circles) reciprocal connections. In **A**, there is no external input, in **B**, there is inhibitory input to the inhibitory unit. **C-D.** The nullclines and vector fields are plotted as in Figure 7.5. Notice the similarity to the oscillator of Figure 7.5B, yet in this case the fixed point where the nullclines cross is stable. In **D**, the inhibitory input lowers the nullcline for r_2 (dotted), that is, reducing r_2 for any fixed level of r_1 , but with the consequence that the crossing point of the two nullclines is raised, producing increased r_2 as well as increased r_1 . **E.** The firing rates settle at the fixed point in the absence of external input. **F.** The firing rates settle to the higher fixed point (increased rate for both units) when the inhibitory unit is inhibited. The code to produce these results is “vector_field.m”. Parameters are $W^{EE} = 2.25$, $W^{EI} = 1.5$, $W^{IE} = -2.25$, $W^{II} = -1$, $\theta_1 = -20\text{Hz}$, $\theta_2 = -15\text{Hz}$, with $r^{(\max)} = 60\text{Hz}$ for both units, $\tau = 10\text{ms}$ and otherwise linear f-I curves as in Eq. 7.4.

Without such stabilization, a system which satisfies the first two requirements is likely to oscillate—indeed, such is the case for the circuit shown in Figure 7.5B, which fulfills the first two requirements, but not the third. The necessary stabilization can arise with nullclines identical to those of Figure 7.5B, if the time constant for inhibitory response is reduced to be faster than that for excitatory feedback. Alternatively, stabilization can arise with different parameters, so that the two nullclines cross in a manner that is qualitatively the same, but with different gradients (Figures 7.6C-D). If the fixed point is stabilized then its position indicates the steady state of the system and an input-driven shift in the fixed point determines the system's response to inputs.

The response of an inhibition-stabilized network to input can be puzzling at face value. In particular, the first so-called “paradoxical” effect is that the stable firing rate of the inhibitory neurons changes in the opposite direction to that produced by any direct input to them. For example, in Figure 7.6, we show that the circuit, in the absence of input, has a stable set of low firing rates. However, if the inhibitory neurons are provided with inhibitory input—which would normally decrease their firing rate—the network feedback causes both the excitatory and the inhibitory neurons to increase their rate. Thus, the response of inhibitory neurons to inhibitory input is an increase of rate and conversely, if they were provided with excitatory input, their rate would decrease.

Such puzzling behavior can be explained graphically in Figure 7.6. If we compare the nullcline for the inhibitory unit, which describes its fixed points if feedback excitation were held fixed, we see that when inhibitory input is added (in Figure 7.6D versus Figure 7.6C) the nullcline moves down, to lower r_2 . However, as it does so, the crossing point of the two nullclines (*i.e.*, the fixed point) moves up, to higher r_2 , as well as higher r_1 .

The intuitive (rather than graphical) explanation is that the dominant input to the inhibitory neurons is from the local excitatory neurons in the feedback circuit. If the direct external input causes the inhibitory neurons to reduce their firing rate, the local excitatory cells over-respond to reduced inhibition by firing a lot more. The increased excitatory activity is more than sufficient to raise the inhibitory rate beyond its initial level.

The second so-called paradox then arises—following this increase in excitation and subsequent increase in inhibition, the excitatory units are firing at a higher rate, while receiving more inhibition than before. So why does their rate not decrease again? The answer to this is that they are on the unstable branch of their nullcline, where the increased direct excitatory feedback they are receiving at high excitatory rate compensates for the increased indirect inhibitory feedback they receive at this rate.

7.3.3. How inhibitory feedback to inhibitory neurons impacts stability of states

For excitatory units, any excitatory feedback increases the effective time constant for decay of activity in the circuit (*cf.* the text following Eq. 6.14). The converse for inhibitory units is that inhibitory feedback causes a more rapid decay of activity following a transient increase, corresponding to a decrease in the effective time constant. Recall also, that slow inhibitory feedback is more likely to engender oscillations, whereas fast inhibitory feedback is more likely to clamp down and stabilize any set of firing rates. The net result in a circuit with reciprocal excitatory and inhibitory feedback is that the stronger the inhibitory-to-inhibitory connections, the more likely a stabilized state arises, whereas the weaker those connections, the more likely oscillations or bistability arise.

7.4. Tutorial 7.1. The inhibition-stabilized circuit.

Neuroscience goals: understand how constant input current can shift a circuit into the inhibition-stabilized regime; understand how bistability can arise between states of low firing rate.

Computational goals: gain more experience at connecting circuits and simulating firing-rate models with different types of f-I curve; using the sign function and ensuring bounds in rate.

In this tutorial, you will produce a model of an excitatory unit coupled to an inhibitory unit using a firing-rate model for each unit's activity. The excitatory unit will have a quadratic firing rate curve, which has the interesting property that its gradient is low at low rates, meaning the effective excitatory feedback can be relatively weak and lead to stability, whereas the gradient increases at high rates, increasing the effective excitatory feedback to a point of instability. Thus, this circuit requires inhibition for stability at high rates—where it can be in an inhibition-stabilized regime—but not at low rates. Such a situation appears to be the case in the circuitry of visual cortex⁹. You will also see how the dynamical regime of the circuit depends on the time constants. In Part B, you will couple together two such excitatory-inhibitory pairs to produce a bistable circuit with distinct states of low activity.

PART A

Simulate the activity of an excitatory unit of rate r_E , coupled to an inhibitory unit of rate r_I (as in Figure 7.6A). The firing rates follow respectively:

$$\begin{aligned}\tau_E \frac{dr_E}{dt} &= -r_E + \alpha_E (I_E - \Theta_E)^2 \cdot \text{sign}(I_E - \Theta_E) \\ \tau_I \frac{dr_I}{dt} &= -r_I + \alpha_I (I_I - \Theta_I),\end{aligned}$$

with the conditions $0 \leq r_E \leq r_{max}$, $0 \leq r_I \leq r_{max}$, which you must enforce. The `sign()` function (use `sign` in Matlab) returns the sign of the quantity within parentheses as ± 1 , and the total currents to each unit are given by:

$$\begin{aligned}I_E &= W^{EE} r_E + W^{IE} r_I + I_E^{(App)} \\ I_I &= W^{EI} r_E + W^{II} r_I + I_I^{(App)}.\end{aligned}$$

The f-I curves and the connection strengths are fixed through all questions in Part A, so the following parameters should be set: maximum firing rate, $r_{max} = 100\text{Hz}$; threshold of excitatory (E-) cells $\Theta_E = -5$ (so their spontaneous rate is 5Hz); threshold of inhibitory (I-) cells, $\Theta_I = 0$; gain of E-cells, $\alpha_E = 0.05$; gain of I-cells, $\alpha_I = 1$; E-to-E connection strength, $W^{EE} = 2$; E-to-I connection strength $W^{EI} = 2.5$; I-to-E connection strength, $W^{IE} = -2.5$; and I-to-I connection strength, $W^{II} = -2$.

In each question, you will simulate the system with given baseline currents (with units in Hz, based on the firing-rate change they cause), which are incorporated as $I_E^{(App)}$ and $I_I^{(App)}$. In a total simulation of 3s, you should apply an extra current to increase $I_I^{(App)}$ by 20 in the middle of the simulation with onset at 1s and offset at 2s. That is $I_E^{(App)}(t) = I_E^{(base)}$ and $I_I^{(App)}(t) = I_I^{(base)} + I_I^{(stim)}(t)$ where $I_I^{(stim)}(t) = 20$ if $1 < t \leq 2$, otherwise $I_I^{(stim)}(t) = 0$.

In each question, explain the system's behavior before, during, and after the extra positive applied current to the inhibitory cells.

- 1) Simulate the system in a default condition with parameters $I_E^{(base)} = 0$, $I_I^{(base)} = 0$, $\tau_E = \tau_I = 5\text{ms}$.
- 2) Simulate the system with increased baseline current, $I_E^{(base)} = 25$, $I_I^{(base)} = 15$, $\tau_E = \tau_I = 5\text{ms}$. (During the stimulus $I_I^{(App)}$ is still increased by 20, so becomes 35).
- 3) & 4) Respectively repeat 1) and 2) but with altered time constants such that $\tau_E = 2\text{ms}$ and $\tau_I = 10\text{ms}$.

Be sure to comment on any differences in the results for questions 1) to 4).

PART B

Duplicate the circuit of Part A so that there are two independent pairs, each pair comprising two units, one excitatory and one inhibitory, with the dynamics provided in Part A. Add two connections between the pairs, from the excitatory unit of each pair to the inhibitory unit of the other pair, with a value $W_{EI-X} = 1.75$ (keep all within-pair connections unchanged from Part A).

- 5) Simulate the system for 3s, applying a pulse of additional excitation, $I_I^{(App)} = 10$, to the first inhibitory unit for a duration of 100ms at the 1-second time-point, and applying such a pulse of excitation to the second inhibitory unit for a duration of 100ms at the 2-second time-point.

For this simulation set $I_E^{(base)} = 25$ and $I_I^{(base)} = 20$, with $\tau_E = \tau_I = 5\text{ms}$.

Explain the resulting activity of the network. How many stable states do you believe the system possesses and describe each of them (giving the set of firing rates of any fixed point). Test that each is stable by, for example, perturbing them by a small amount with an applied current or adding a small amount of noise.

7.5. Attractor state itinerary

Box 7.7. Attractor state itinerary: The process of a system changing from the vicinity of one “quasi-stable” fixed point to another, typically with dwelling periods in the vicinity of each fixed point being longer than the times taken to transition between them.

Neural activity *in vivo* is notoriously variable, which is why many trials with identical stimuli are needed to build up a reliable picture of the neural responses¹⁰. Such variability appears to be at odds with any theory of information processing based on attractor states, in particular the fixed-point attractors discussed so far. However, if neural activity “jumps” between different, distinct attractor states—a process called attractor state itinerary¹¹—the spike times of single neurons would be highly variable. Moreover, if the timing of such jumps were unreliable, varying from trial to trial, then the rapid transitions between states

may not be revealed when spike trains are averaged across trials according to standard procedures. In Chapter 9 we consider methods that do not rely upon trial-averaging for analysis of neural activity patterns, so could reveal any such attractor state itinerary. Here we consider a simple model of one of the more likely occurrences of attractor state itinerary.

7.5.1 Bistable Percepts

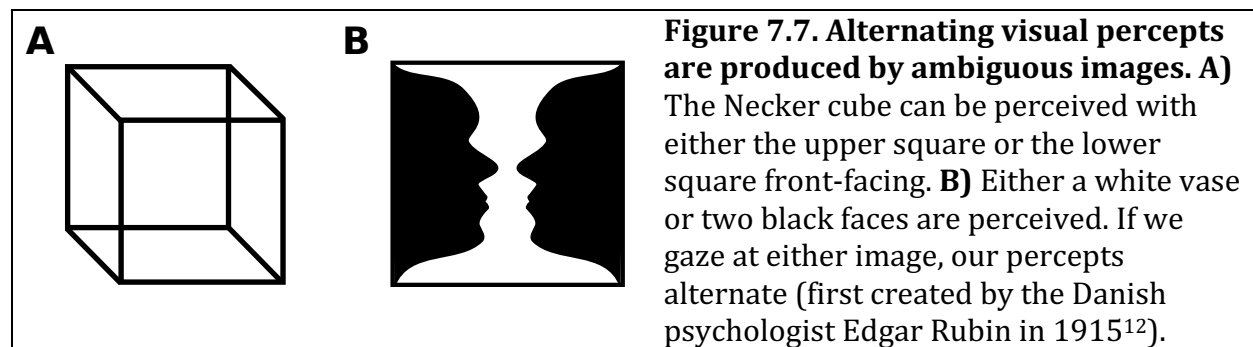


Figure 7.7. Alternating visual percepts are produced by ambiguous images. **A)** The Necker cube can be perceived with either the upper square or the lower square front-facing. **B)** Either a white vase or two black faces are perceived. If we gaze at either image, our percepts alternate (first created by the Danish psychologist Edgar Rubin in 1915¹²).

As we saw in Section 5.7, the Necker cube (Figure 7.7A) is one of many examples of visual image that can be perceived in more than one way (see also Figure 5.8). If we stare at the Necker cube, initially one of the squares appears to be the closest face. However, after a few seconds the cube appears to switch orientation, with what was previously a rear-face becoming the closest face. The times between such transitions are variable and their distribution enables us to gain some insights into the underlying neural processes that cause such transitions¹².

Box 7.8. Perceptual rivalry: A phenomenon in which a single stimulus can be perceived in more than one manner, causing a switching back and forth between these different percepts.

Studies of transitions between dominant percepts—or perceptual rivalry—can arise when different images are presented to the two eyes (binocular rivalry^{13,14}), or when a subject views moving oriented plaids, where two sets of parallel stripes move across each other at an angle^{15,16}. In the case of moving plaids, percepts of up-down motion, or left-right motion, or a coherent motion of diamonds formed by combining the two sets, are all possible. The widths, contrasts, and orientations relative to direction-of-motion, all contribute to determining the distribution of durations of each percept in between transitions.

Auditory stimuli can also provide bistable percepts^{17,18}—sequences of tones of different frequencies can be perceived as a single stream or as distinct sources. It would be interesting to find such stimuli in other modalities, such as smell, taste, or touch.

It is relatively easy to produce ambiguous percepts in the visual domain because we perceive a three-dimensional world, while our eyes only receive a two-dimensional projection of the world around us. It is perhaps the combination of such inherent ambiguity with the greater extent of model-building of the visual domain within our brains—and the

concomitant attractor states underlying such models—that renders visual sensory inputs the most likely to produce attractor state itinerancy.

7.5.2 Noise-driven transitions in a bistable system

If a dynamical system, such as a neural circuit, possesses two fixed points, a transient external input can cause a transition from one fixed point to another (Figure 6.4B). Random fluctuations of an input that is in the form of zero-mean white noise can cause transitions in a similar manner. In the latter case then the time spent in one state before a sufficiently large noise-fluctuation knocks the system into the other state is highly unpredictable and follows a near-exponential distribution (Figure 7.8B,E). In fact, in the limit that the time between transitions is much longer than the time to actually make the transition (so most of the time is spent “waiting” for a large noise fluctuation) the state-transitions follow a Poisson process, which has an exponential distribution of intervals between transitions (Section 3.3.3). In general, an analysis of the distributions of state durations (Figure 7.8D-F)

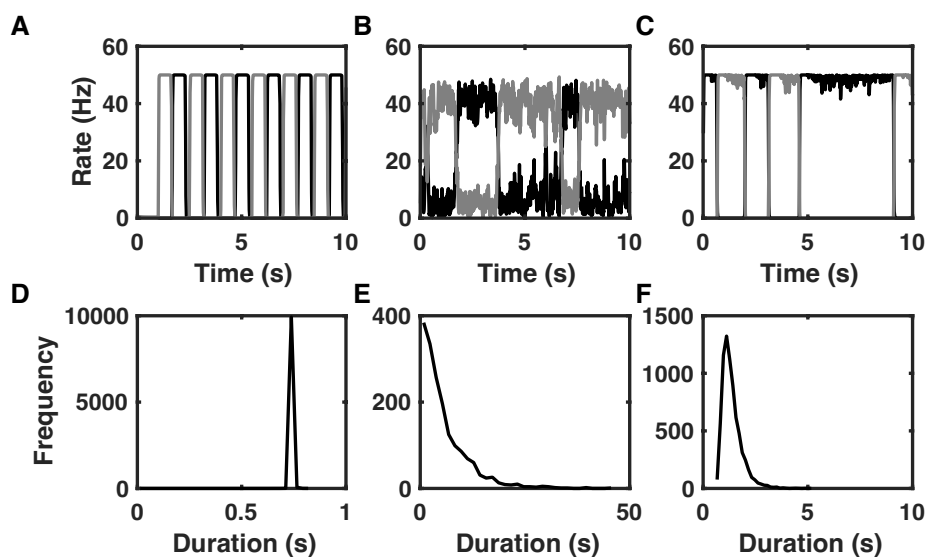


Figure 7.8. Transitions between attractor states in a bistable system. **A.** An adaptation current is added to the winner-takes-all network of Figure 6.8. The time for the adaptation current to build up in the highly active unit depends on that unit’s firing rate, while the time for the adaptation to decay in the silent unit is equal to the time constant (of 250ms in this example). The resulting switching of the dominant unit is periodic, with near-identical state durations (D). **B.** Instead of an adaptation current, external noise is added to both units in a bistable winner-takes-all network. State durations (times between transitions) are highly variable, producing an exponential distribution (E). **C.** A combination of weaker adaptation current and weaker noise produces variable state durations. Very brief state durations are rare because the adaptation must build up enough for the noise to have a significant chance of causing a transition. The resulting shape of the distribution of state durations (F) matches that of percept durations during perceptual rivalry tasks²⁰. **D-F**) The distribution of the number of occurrences of different state durations over 10,000 sec trials of the activity shown in A)-C) respectively. The code to generate this figure is `bistable_percept.m`.

can provide strong evidence for a particular architecture of the underlying neural circuitry²¹.

7.6. Quasi-steady states and relaxation oscillators: the FitzHugh-Nagumo model

If one variable of the system changes slowly enough compared to other variables, the system can be analyzed with the slow variable treated as a fixed parameter that determines the available states of the system. Once the available states are found assuming a fixed slow parameter, then the slow variable is allowed to gradually vary. As the slow variable gradually varies, so too do the available states, until a bifurcation point is reached where the system's current activity state loses stability.

Box 7.9. Quasi-steady state: A state of a system, which is almost stable and appears stable for a duration longer than the system's fastest timescales, but eventually proves to be unstable.

Box 7.10. Relaxation oscillator: A system which regularly switches between different quasi-steady states, with long durations within each state compared to the timescale of more rapid jumps between those states.

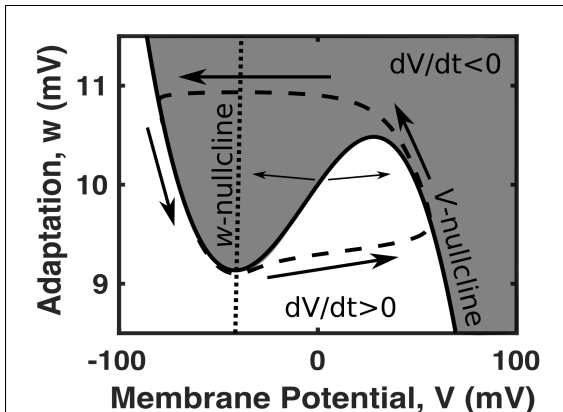


Figure 7.9. The FitzHugh Nagumo model.

The cubic V -nullcline (solid line) separates regions where $\frac{dV}{dt} > 0$ (unshaded) from regions where $\frac{dV}{dt} < 0$ (shaded gray). When the system is oscillating, (dashed trajectory) it changes slowly when its variables lie on or near the V -nullcline, but it jumps rapidly (horizontal arrows) between the high- V and low- V branches of the nullcline when the system reaches the bifurcation points (maxima and minima of the V -nullcline). In this manner, the membrane potential cycles around the range of adaptation, w , where, if w were fixed, V would be bistable. This

figure was produced by the online code
FHNmodel.m.

If multiple attractor states are present in the system with the slow variable fixed then interesting behavior resembling attractor state itinerancy can arise when the slow dynamics of that variable are included. For example, the attractor states may slowly change until the one corresponding to the system's activity becomes unstable—in which case the state was “quasi-stable”, not completely stable. The activity will then rapidly change to reach a new quasi-stable attractor state. The time between the system's transitions from one attractor state to another is the time taken for the attractor state to become unstable, which depends on how rapidly the slow variable changes. We saw an example of such behavior in Figure 7.8A, where the slow adaptation variable changes more than an order of magnitude more slowly than neural firing rates. The resulting behavior in a two-state

system can be periodic—as it is in Figure 7.8A—in which case the system is a type of oscillator called a relaxation oscillator.

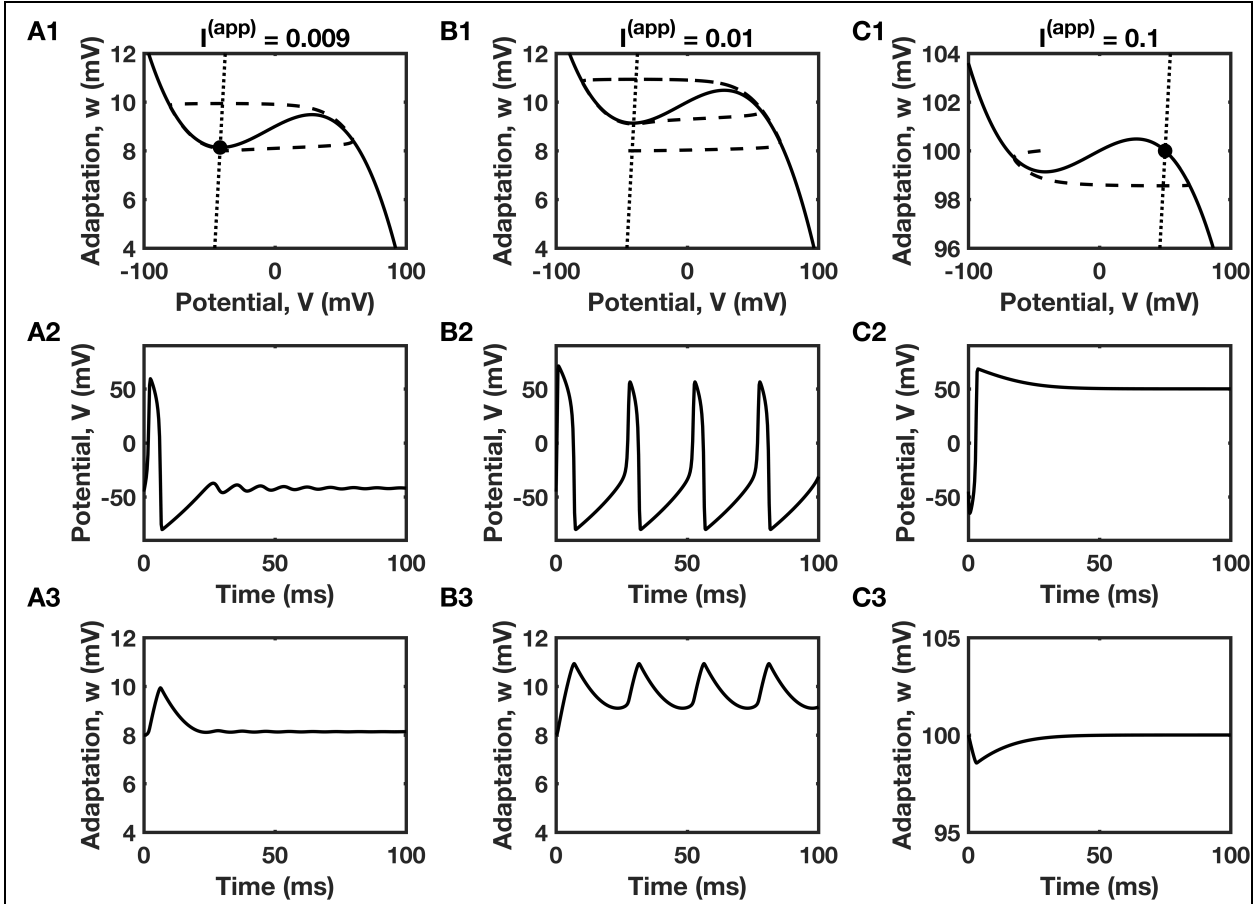


Figure 7.10. The FitzHugh-Nagumo model behaves like a Type-II neuron. **A.** With small applied current, $I^{(app)} = 0.009$, a single spike occurs, followed by subthreshold oscillations. **A1.** Nullclines are shown with $\frac{dV}{dt} = 0$ solid and $\frac{dw}{dt} = 0$ dotted. The trajectory of $w(t)$ versus $V(t)$, dashed, depicts the spike as a single orbit jumping between stable sections of the V -nullcline, but ultimately resting at the stable fixed point (solid circle) where the two nullclines intersect. **A2.** Membrane potential versus time and **A3**, adaptation variable versus time for the same applied current of $I^{(app)} = 0.009$. **B.** With a larger applied current, $I^{(app)} = 0.01$, the V -nullcline shifts up to higher values of w (**B1**) and regular spiking occurs (**B2**), with repeated loops between the higher and lower branches of the V -nullcline followed. Axes of B1-B3 are identical to those of A1-A3. **C.** With very large applied current, $I^{(app)} = 0.1$, the w -nullcline intersects the V -nullcline on its upper branch, producing a stable fixed point at high membrane potential. Spike-like oscillations are no longer possible. Axes in C1-C3 are shifted to higher values of w . The figures depict solutions of Eq. 7.7, with parameters $V_0 = -50\text{mV}$, $V_1 = -70\text{mV}$, $V_2 = 50\text{mV}$, $\beta = 8$, $\tau_V = 0.01\text{ms}$, $\tau_w = 200\text{ms}$, and the applied currents shown. This figure was produced by the online code FHNmodel1.m.

One of the best-known examples of a relaxation oscillator is the FitzHugh-Nagumo model⁴⁻⁶, which is a two-variable simplification of the Hodgkin-Huxley model, capable of reproducing and explaining many of its Type-II properties (Section 4.2.3).

The two variables in the FitzHugh-Nagumo model are the membrane potential, V , and an adaptation variable, which is given the symbol w . The key ingredient of the model is the cubic dependence of the rate of change of membrane potential, $\frac{dV}{dt}$, on membrane potential, V . Such a cubic dependence matches the shapes of the $\frac{dr}{dt}$ equation in Figures 7.1 and 7.2, which we saw can lead to bistability. As in other single neuron models, $\frac{dV}{dt}$ increases with applied current, I , which shifts up the curve of $\frac{dV}{dt}$ versus V , and decreases with adaptation, which shifts down the curve of $\frac{dV}{dt}$ versus V . This means that at fixed high levels of adaptation only lower values of membrane potential can be stable, at fixed low levels of adaptation only higher values of membrane potential can be stable, whereas at fixed intermediate levels of adaptation both lower and higher values of membrane potential can be stable (see Figure 7.9).

The ODEs describing a general form of the FitzHugh-Nagumo model are:

$$\begin{aligned}\tau_V \frac{dV}{dt} &= -\beta V(V - V_1)(V - V_2) - w + I^{(app)} \\ \tau_w \frac{dw}{dt} &= V - V_0 - w,\end{aligned}\quad \text{Eq. 7.7}$$

where V_1 and V_2 determine the range of membrane potential variation, V_0 is the membrane potential above which the adaptation variable rises above zero, β determines how much adaptation is needed to cause a jump in V , τ_V is a very short time constant that determines the rate of rapid upswing and reset of membrane potential during a spike, τ_w is a much longer time constant, which determines the rate of recovery between spikes and the spike-width, and $I^{(app)}$ is the applied current in units of the voltage-change it would cause in the absence of the spike mechanism.

The separation of timescales ($\tau_V \ll \tau_w$) ensures that the system spends most of its time on the V -nullcline, given by $\frac{dV}{dt} = 0$. This cubic nullcline is given by the equation

$$w = -\beta V(V - V_1)(V - V_2) + I^{(app)}, \quad \text{Eq. 7.8}$$

and plotted in Figure 7.9. Whenever w is less than this value (below the curve in Figure 7.9, unshaded region) then Eq. 7.7 shows us that $\frac{dV}{dt} > 0$, so the membrane potential increases rapidly and the trajectory moves to the right until it hits the V -nullcline, where Eq. 7.8 is satisfied.

When Eq. 7.8 is satisfied, so that the system rests on the V -nullcline, then according to Eq. 7.7, the adaptation variable slowly changes, increasing if $w < V - V_0$ (while to the right of the w -nullcline) and decreasing if $w > V - V_0$ (while to the left of the w -nullcline). Therefore, with the parameters that produce Figure 7.9, when the membrane potential is at its high level, adaptation increases until it is so high that the high- V branch of the V -nullcline disappears. Once there is no longer a stable state of high membrane potential, the membrane potential rapidly drops until the system is on the low- V branch of the V -nullcline. When the system is on the low- V branch of the V -nullcline, the adaptation variable decreases, until the membrane potential no longer has a stable low value, in which

case the membrane potential rapidly jumps to the high- V branch of its nullcline to initiate a spike. The process repeats to produce oscillations (Figure 7.10B).

7.7. Heteroclinic sequences

Box 7.11 Saddle point. A fixed point, which is stable in at least one direction but also unstable in at least one direction. Given the impossibility in practice of having no motion in the unstable direction, saddle points are overall unstable, but they can be approached before being departed from. The system can reside near the saddle point for a long time.

Box 7.12. Heteroclinic sequence. A trajectory of a dynamical system that passes from one saddle point to another, typically with long times of relative constancy near each saddle point interspersed with rapid changes in the variables as the system processes between saddle points.

We have so far considered fixed points that are either stable (so produce attractor states) or unstable. We have also considered the marginal stability of a line attractor (Section 6.3.5). In systems with more than one dimension (*i. e.*, in any system with multiple variables) unstable fixed points can be saddle points—there can be directions from which the network’s activity moves toward the fixed point, as well as directions in which the network’s activity moves away from the fixed point. That is, depending on the set of values of all variables, the activity approaches or departs from a fixed point. The unstable fixed points of Figure 7.5A are examples of saddle points, with a clearer example provided in Figure 7.11.

High-dimensional systems, like those comprised of many neurons or units, with a great deal of heterogeneity in their interconnections, are likely to possess many saddle points^{22,23}. In such cases the system’s activity can process from the vicinity of one saddle point to another, producing a heteroclinic sequence²⁴. If the activity returns to the vicinity of the original saddle point then repeats, a heteroclinic orbit is produced.

A heteroclinic sequence can appear to have near-stationary activity while in the vicinity of a fixed point (*cf.* Figure 7.11 D-E). Moreover, the time spent near the fixed point depends on how closely the activity approaches the fixed point (as without noise, if the system ever reached the fixed point precisely, it would remain there forever). Therefore, while multiple trials with small differences in initial conditions can lead to a reproducible sequence of states, each state being the activity at a fixed point, the time spent in those states can vary. In this sense, the heteroclinic sequence can resemble a series of noise-driven transitions between discrete attractor states¹¹.

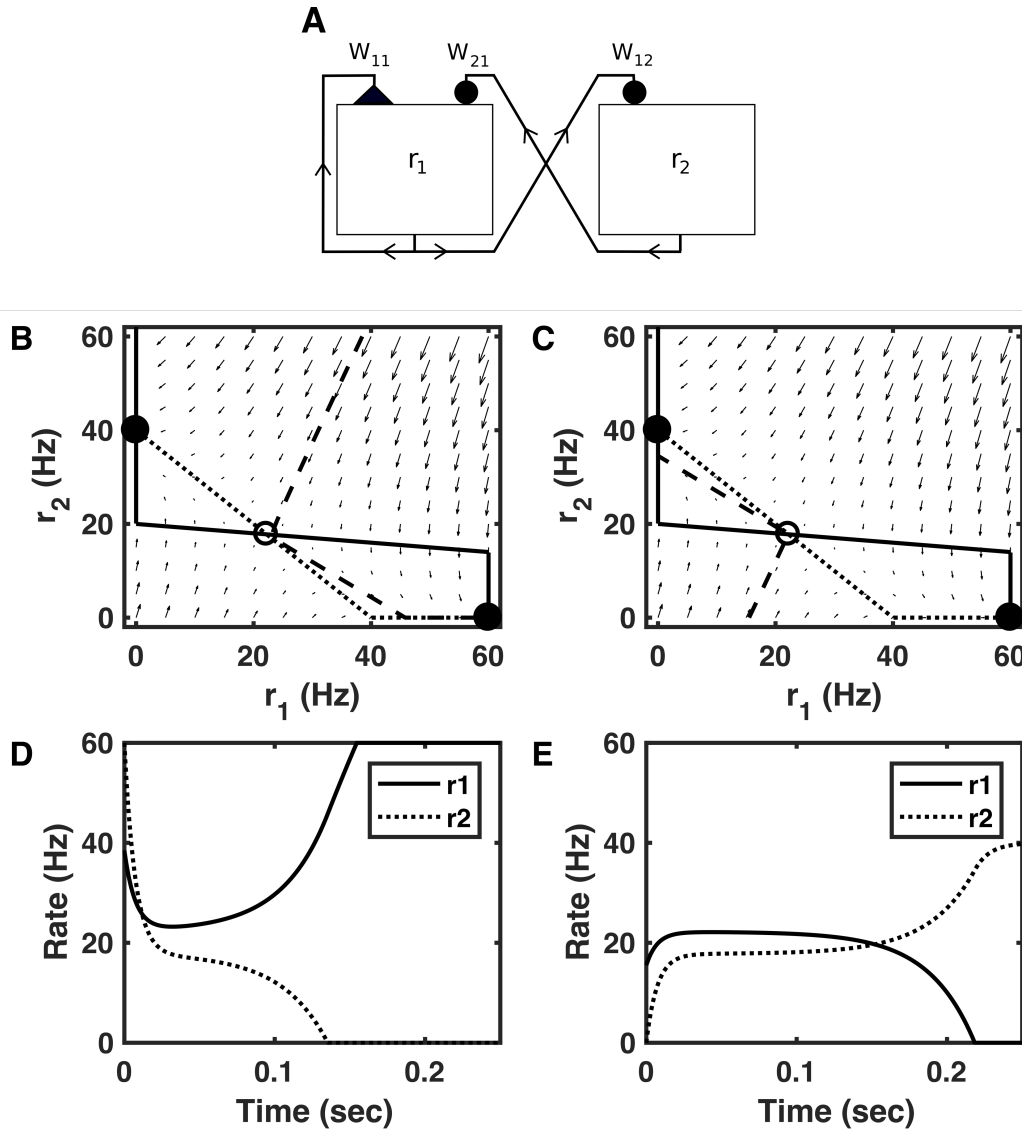


Figure 7.11. Example of a saddle point in a circuit with cross-inhibition. **A.** Circuit architecture with cross-inhibition between two units similar to that of a decision-making network (Section 6.5) (solid circles = inhibitory connections; triangle = excitatory connection). **B-C.** Nullclines cross in three places with stable fixed points shown as solid circles and the intermediate unstable fixed point, which is a saddle point, as an open circle. Arrows indicate direction of change of the system's firing rates. Dashed lines are trajectories, which initially approach the saddle point then deviate to one of the stable fixed points. **D-E.** The firing rate curves that correspond to the trajectories in B and C respectively. Note the period of slower rate of change and the non-monotonic variation of one of the firing rates, a hallmark of approach toward then departure from a saddle point. The code to produce these results is “vector_field_saddle.m”. Parameters are $W_{11} = 0.95$, $W_{12} = -1$, $W_{21} = -0.5$, $\Theta_1 = -10\text{Hz}$, $\Theta_2 = -40\text{Hz}$, with $r^{(\max)} = 60\text{Hz}$ for both units, $\tau = 10\text{ms}$ and otherwise linear f-I curves as in Eq. 7.4.

7.8. Chaos

Perhaps the best-known example of a chaotic system is the atmosphere, with its weather patterns being notoriously unpredictable beyond a few days in many parts of the world. Indeed, one of the criterion of chaos is epitomized in the “butterfly effect”, so-called because the tiniest perturbation, such as the flutter of a butterfly’s wings, could make the difference between a hurricane hitting one continental region or another a week later. Mathematically, chaotic systems have such strong sensitivity to initial conditions that the impact of a tiny effect grows exponentially over time. The high variability of neural firing *in vivo*—a variability that can be reduced by input from a stimulus^{25,26}—is suggestive that the cortex operates in a chaotic state.

In an unstable single-variable system—such as one of exponential growth—the effect of a small change at one point in time can be exponentially magnified as time progresses, but such systems are not chaotic. Therefore, a second criterion is needed to define a chaotic system, namely the requirement of mixing of trajectories. For example, if the system is changed by a small increase in one variable, then for the system to be chaotic, as that variable changes through time at some point it must become less than what it would have been without the initial increase. For this condition to be satisfied, it turns out that chaotic systems must be nonlinear and contain at least three variables².

Box 7.13. Chaotic system: A system whose behavior is extremely sensitive to initial conditions, with diverging trajectories that remain bounded and cross over each other in any 2D projection.

Box 7.14. Edge of chaos: A system operating with a set of parameters, which if adjusted in one direction cause the system to be chaotic, while if adjusted in the other direction causes the system to have stable states. The particular set of parameters can be called “critical” and the system may exhibit criticality.

Box 7.15. Criticality: The property of a system with fluctuations on all length scales and time scales, typified by power-law exponents in the distributions of measured properties, such that measurements of the system at different length scales or time scales generate qualitatively similar results to each other.

7.8.1. Chaotic systems and lack of predictability

The exquisite sensitivity to initial conditions of a chaotic system leads to its behavior, just like the weather, being unpredictable beyond a small period of time. It may seem that such unpredictability should be avoided in neural circuits that control our behavior and responses to the environment—if we see a red stop light ahead of us when driving, we would hope that our foot reliably presses the brake pedal. However, initially chaotic systems can be trained to produce reliable responses (*i. e.*, with small changes in connections they are shifted out of the chaotic regime), so long as they are not initially “too chaotic”^{27,28}. It is likely that, with their vast repertoire of internal dynamics, when operating near the “edge of chaos”²⁹, chaotic systems are the most versatile when it comes to training a circuit to produce a novel, arbitrary response³⁰.

As a source of unpredictability, moreover, chaos could be beneficial. Just as evolution relies on random variation to produce differences in genetic expression that occasionally might be favorable (and then propagated), so too can random variability in our responses to the environment allow us to explore alternative behaviors. If those alternative behaviors prove to be beneficial, we would want them to be reinforced so that we are more likely to repeat them in similar circumstances. Such reinforcement is an aspect of learning that we will consider in Chapter 8, but for here the key point is that random variation of behavior or strategy when faced with a decision or task is an important step in achieving an optimal response. In this context, the random variation is known as exploration.

Unpredictability is also beneficial in the competitive systems explored by game theory³¹. For example, if you are a potential prey, then if your actions are completely predictable ahead of time, a predator can lie in wait and obtain an easy meal. If our actions, at least at the large scale, were based on the state of a chaotic system, we would be much harder to catch.

While the unpredictable behavior of a chaotic neural circuit may therefore be beneficial, such unpredictability need not arise from the sort of chaos that we consider here.

Neural activity *in vivo* is indeed unpredictable on a trial-by-trial basis, particularly at the low level of individual neural spikes, as would be expected in a chaotic system. However, such unpredictability need not arise from the sort of chaos that we consider in this book—that is, chaos arising from the coupled differential equations reflecting neural firing rates, or the interaction between membrane potentials and conductance of various channels. Rather, it is also possible that the observed variability is accounted for by a combination of environmental fluctuations and microscopic noise sources within the brain.

Microscopic noise arises from the motion of molecules—a motion, which in of itself is chaotic—driven by thermal energy. Microscopic noise may seem a very unlikely source of variability in the behavior of an animal weighing over 100 pounds, given the law of large numbers: random variations at the microscopic level tend to cancel out on a large-scale, so rocks do not suddenly jump off the ground (as they might if all of the air molecules hitting them ever did so in a concerted fashion). Yet neural systems appear to be fashioned so that there are many “points of no return” or “all-or-none” effects, from vesicle release to a neural action potential, to a transition between attractor-states of neural activity. These “all-or-none” effects can occur in subsystems with few molecules (*e.g.*, the number of proteins that must be bound near an axon terminal to ensure a vesicle’s release) or few components of the next sub-cellular scale (*e.g.*, the number of release-ready vesicles at a synapse). Each “all-or-none” event amplifies noise at a small scale to a larger scale. All of these amplifications can combine to allow a tiny fluctuation at the microscopic level to increase to a level that produces a change in behavior.

Box 7.16: Deterministic: A system in which the dynamics are fully determined given the differential equations it follows, combines with its initial conditions—*i.e.*, no randomness is added.

In many of our prior simulations, we have included such microscopic noise via random numbers. By contrast, when we discuss chaos in a neural system, we typically ignore such low-level noise and study the random-looking behavior that arises from deterministic coupled differential equations. The subtlety of deterministic chaos is that although at each time-step the values of variables are completely determined by their values in the prior time-step (as in all of the ODEs we have solved without an additional random noise term) the values of the variables many time-steps ahead cannot be determined with any reliability if their current values are not known with infinite precision—a precision that is practically impossible in all scenarios outside of a computer or mathematical equation.

7.8.2 Examples of chaotic neural circuits

We will consider first an example of a chaotic three-variable system. The system produces the simplest type of chaos, based on near-oscillatory behavior of three firing-rate model units. Later in the section we will consider a system with many more firing-rate units, whose chaotic behavior is high-dimensional, so appears more like the “chaos” of everyday use, containing no obvious patterns.

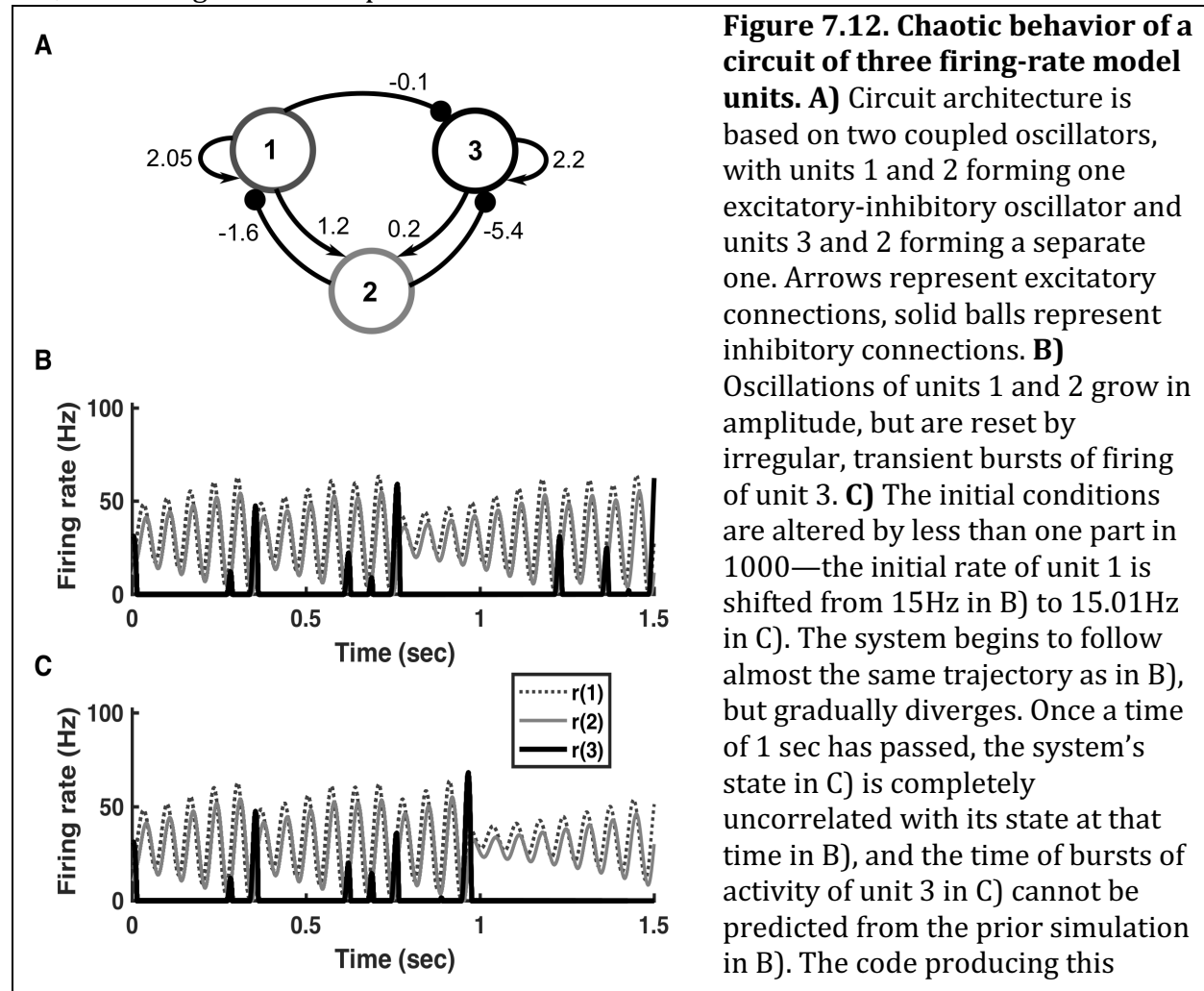


figure can be found online as
chaotic_3units.m.

Chaotic systems with few variables can arise when oscillators become unstable through a parameter shift (*e.g.*, if a modulator alters a conductance, or if a synaptic connection changes) or through an interaction with another oscillator. Remnants of the underlying oscillator are visible in the behavior of these low-dimensional chaotic systems, as is the case of the model neural circuit shown in Figure 7.12. Office toys, sometimes called kinetic sculptures, with a driven magnetic pendulum connected to a second arm that is able to rotate in either direction have similar behavior (*e.g.*, those sold as “Mars” or “Jupiter”) with the direction of motion of the central arm becoming rapidly unpredictable.

In Figure 7.12 we show that a connected circuit of three firing-rate units—in this example, with firing-rate curves that are linear, combined with a threshold and a maximum rate—can be chaotic. The structure of the circuit is such that units 1 and 2 alone produce an oscillator based on self-excitation within unit 1 that receives inhibitory feedback via unit 2. Units 3 and 2 together produce a similar, though slightly less excitable, oscillator. No noise source is added to the system, but the times of switches—when the dominant oscillation of units 1 and 2 becomes temporarily suppressed because unit 3 produces a burst of activity—become rapidly unpredictable. Moreover, an imperceptible change in initial conditions (compare panel C with B) produces a change in activity that diverges more and more from the unperturbed activity as time progresses until the two activity traces (the one with and the one without the perturbation) are completely uncorrelated.

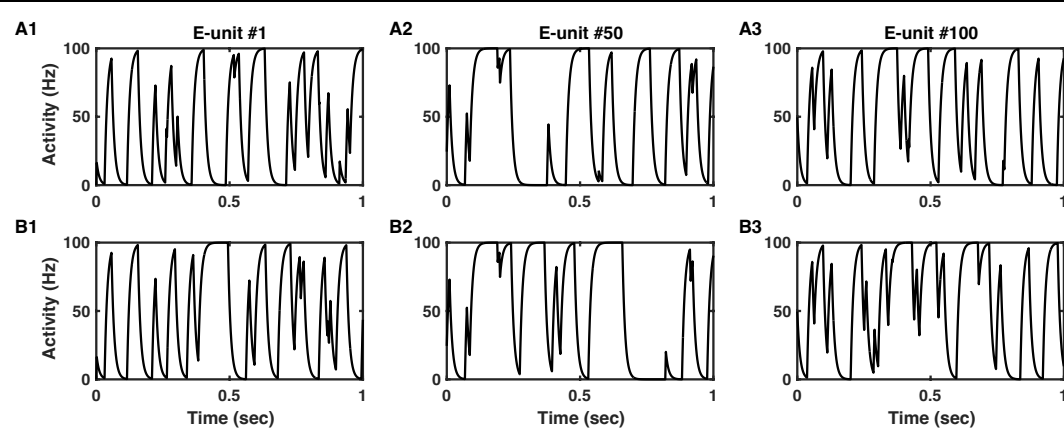


Figure 7.13. Chaotic neural activity in high dimensions. Firing rate as a function of time is shown for three excitatory units selected from a balanced network of 200 excitatory and 200 inhibitory units with sigmoidal firing rate curves and random, sparse connections between units. Unlike Figure 7.12, no vestige of regular oscillation remains in the chaotic activity. **A)** Unperturbed activity with initial rates evenly spaced in the range from 0 to 100Hz. **B)** Perturbed activity with the initial rate of a single unit shifted from 0 to 10^{-14} Hz, while the initial rates of other units remain identical to those in A). The activity in B) initially appears unchanged from that of A), but deviations are visible after a few hundred milliseconds. The timescale of divergence is independent of the particular unit that is

perturbed initially. The code producing this figure can be found online as `highD_chaos.m`.

A system with many more units becomes chaotic if units receive balanced input—in firing rate models this corresponds to a mean current of zero as excitation is matched on average by inhibition—while connection strengths between units exceed a threshold³². Indeed, interest in chaotic behavior of neural circuits was spurred in the late 1980s, by a paper of Sompolinsky and colleagues³³, showing this result for an infinite system via mathematical proof.

Box 7.17: Lyapunov exponent: A measure of the tendency for trajectories of a system to approach each other (a negative exponent, suggestive of attractor states) or diverge from each other (a positive exponent, suggestive of chaos).

The behavior of an example network with 200 excitatory and 200 inhibitory coupled units is shown in Figure 7.13. The sensitivity to initial conditions of this network is so extreme that the rate of a single unit is altered by only 10^{-14} Hz in the lower set of panels (Figure 7.13 B1-3), yet such a microscopic (indeed physically implausible deviation in a firing-rate model) is sufficient to produce a large-scale change in activity within a few hundred milliseconds. If we measure the mean across all 200 excitatory cells of the absolute change in their firing rates caused by the tiny perturbation, we see that the change grows exponentially until the system size is reached (Figure 7.14). Such exponential growth is a hallmark of chaos and the rate of growth, known as the Lyapunov exponent, is positive for a chaotic system—whereas for a system of attractors it would be negative, indicating exponential decay to stable fixed points.

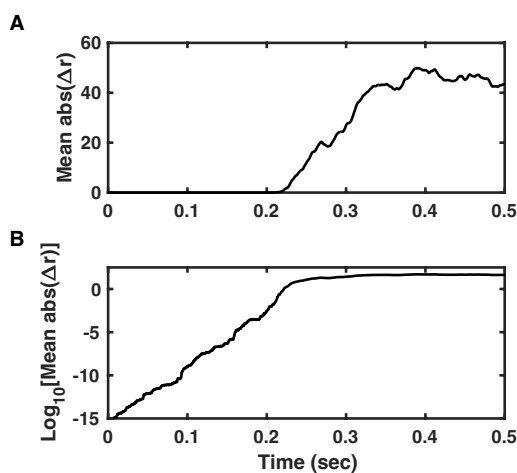


Figure 7.14. The divergence of firing rates grows exponentially following a small perturbation in a chaotic system. **A)** The mean of the absolute difference in firing rates of all excitatory units of the network used to produce Figure 7.13, is plotted as a function of time. The initial perturbation of 10^{-14} Hz in one unit out of 200 corresponds to a mean change of 5×10^{-16} Hz across all units. The change in network activity appears negligible until after 200ms the exponential growth brings the change up to the size of the system. **B)** The logarithm (base 10) of the plot in A) reveals the exponential period of growth as a straight line. The code producing this figure can be found online as “`highD_chaos.m`”.

7.9. Criticality

Criticality is a phenomenon that has been studied intensely and documented abundantly in the field of physics^{34,35} prior to its more recent observation and study in neural circuits^{36,37}.

The main hallmark of criticality is one of correlations that arise on many length scales and time scales. That is, if the system is changed in one place, that change may have a very local effect, or it may propagate to alter the entire system (see Figure 7.15).

As suggested by Figure 7.15, criticality is closely related to the need for the brain to reside in a state in which some but not all neurons fire. If the mean strength of connections between neurons is too weak, or if neurons are not excitable enough, any initial pulse of activity quickly dissipates in neural circuits (Figure 7.15A). Conversely, if connections are too strong and/or neurons are too excitable, any small input leads to runaway excitation with the majority of neurons eventually firing synchronously (Figure 7.15C), which is a symptom of epilepsy. Between these two types of activity, just like at the “edge of chaos”, the brain can maintain activity in a fraction of neurons that most of the time neither grows excessively nor disappears (Figure 7.15B). Typically to achieve such a state, one or more homeostatic processes is required. We will consider such processes in Chapter 8.

Box 7.18. Homeostasis: A point of balance that is a long-term equilibrium for the system, dependent on **homeostatic processes**, which produce such a “Goldilocks effect” of being neither “too hot” nor “too cold”.

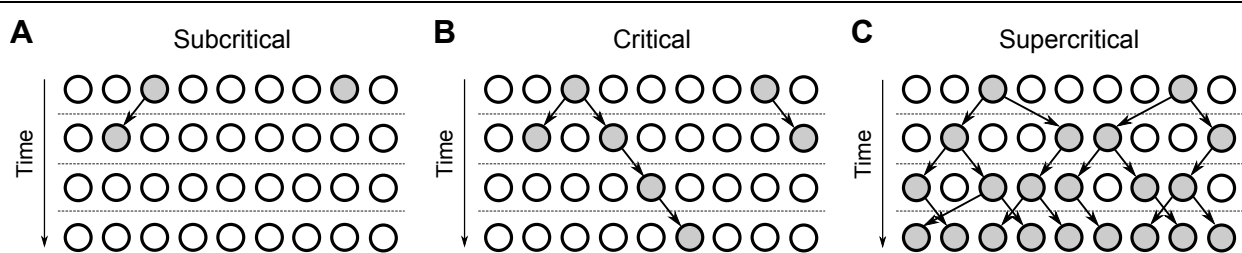


Figure 7.15. Propagation of activity as “avalanches” indicate whether a network is in the critical state. **A)** In a subcritical network, the effect of each spike is to produce, on average, less than one extra spike in all other neurons, so avalanches typically decay. Two avalanches are shown, one of size 2 and duration 2 (on the left), the other of size 1 and duration 1 (on the right). **B)** In the critical state, each spike causes, on average, exactly one extra spike in another neuron, so avalanches can propagate or decay quickly. Two avalanches are shown, one of size 5 and duration 4 (on the left) and one of size 2 and duration 2 (on the right). **C)** In a supercritical network, each spike causes on average more than one extra spike in other neurons, so avalanches commonly propagate and can extend to the full size of the system. The two avalanches initiated in the first time-step merge and quickly reach the system’s size.

It may be intuitive that a system balanced between dissipation and explosion of activity has computational advantages. In particular, the range and number of distinct responses to inputs is greater in a system at a “sweet spot”, where activity can both increase or decrease overall, or simply shift between cells, compared to a system in which most cells respond with high activity or remain silent when receiving input. Critical systems, in which responses can range from the tiny to the macroscopic, provide the largest repertoire of possible responses to initial perturbations. Such a large repertoire of

responses is an indication that a system in the critical state, which can be at the “edge of chaos”³⁸, has a high capacity for information processing.

7.9.1 Power-law distributions

One hallmark of criticality is a power law in the distribution of sizes and durations of avalanches. An avalanche can be defined as a sequence of time bins across which activity exceeds a defined threshold. For example, when a subset of neurons is recorded, the observation of one or more spikes in a series of successive time bins constitutes an avalanche. Alternatively, activity can be measured at a larger scale, either through the local field potential (arising from the shifts in ions averaged across many neurons) or functional magnetic resonance imaging (fMRI, which measures change in blood flow to small volumes called voxels in response to activity of many neurons there). In this case, a threshold level is set and the spatial data is transformed into a set of entries of 1 or 0, with each entry indicating whether the activity level is above or below the threshold at a given location and in a given time bin.

Box 7.19. Avalanche: A measure of neural activity that exceeds a given threshold over multiple successive time-bins.

The duration of an avalanche is then the stretch of time—or number of successive time bins—without loss of activity. The size of an avalanche is the number of total spikes (or distinct activations of sites) during the avalanche. The size of an avalanche can be greater than the system’s size (the number of recorded sites) because reactivation of cells is possible (as in Figure 7.15C). In the critical state, plots of the number of avalanches as a function of their size, the number of avalanches as a function of their duration, and the mean sizes of avalanches as a function of their duration all are best fit by power-laws. Given the characteristic property of logarithms, $\log(x^\alpha) = \alpha \log(x)$, the best way to observe a power-law distribution is to plot the logarithm of the number of occurrences versus the logarithm of the value being measured and look for a straight line.

For example, if the number of avalanches, N , with a given number of spikes, s , follows a power law so that $N = ks^{-\beta}$ then $\log(N) = \log(k) - \beta \log(s)$ so a plot of $\log(N)$ against $\log(s)$ is a straight line with a gradient of $-\beta$. Examples of such plots are shown in Figure 7.16.

Observation of power-law distributions is not sufficient to indicate the presence of criticality. Indeed, many non-critical systems can produce such power laws³⁹. Moreover, it can be very difficult to show that a distribution of avalanches follows a power law, because the range of sizes or durations of avalanches should range over three orders of magnitude for other distributions to be ruled out. It takes a long time to obtain sufficient statistics to compare the relative abundances of avalanches across such a wide range, in particular because the large ones are so rare.

7.9.2 Requirements for criticality

When analyzing the distributions of avalanches, three power laws should be found if the system is critical. The first is the number of avalanches of a given duration as a function of

duration (Figure 7.16A). The second is the number of avalanches of a given size as a function of size (Figure 7.16B). The third is the mean size of an avalanche of a given duration as a function of duration (Figure 7.16C). These power laws have exponents that are defined respectively in the equations below:

$$f_d(T) \propto T^{-\alpha} \quad \text{Eq. 7.9}$$

$$f_s(S) \propto S^{-\tau} \quad \text{Eq. 7.10}$$

$$\langle S \rangle(T) \propto T^{\frac{1}{\sigma\nu z}} \quad \text{Eq. 7.11}$$

where T is the duration of an avalanche, f_d is the number of a given duration, s is the size of an avalanche, f_s is the number of a given size, and $\langle S \rangle(T)$ is the mean size of a given duration. The three exponents, τ , α , and $\frac{1}{\sigma\nu z}$ (the last one appears to have three variables within it, based on the theory of critical systems, but is treated as a single exponent) should be measured separately from fits to log plots of the avalanche distributions.

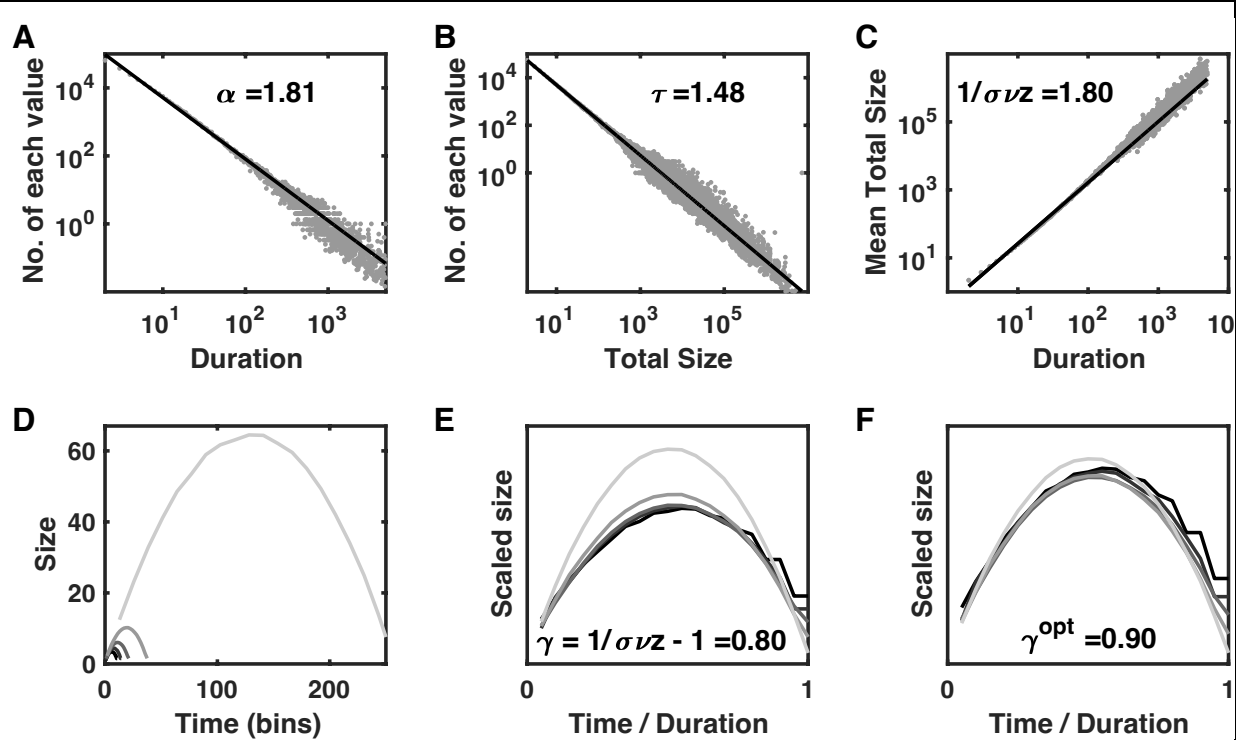


Figure 7.16. Analysis of avalanche data from a simple ‘birth-death’ model of neural activity. **A)** A log-log plot of the number of avalanches as a function of avalanche duration. Gradient of the straight line yields α , the exponent of the power-law. **B)** A log-log plot of the number of avalanches as a function of the total size of the avalanche. Gradient of the straight line yields τ , the exponent of the power-law. **C)** A log-log plot of the mean size of avalanches as a function of their duration (*i.e.*, x-values of panel B, plotted against x-values of panel A). Gradient of the straight line yields $\frac{1}{\sigma\nu z}$, the exponent of the power-law. However, in this case the scaling relation of a critical system is not quite satisfied, as $\frac{1}{\sigma\nu z} = 1.80 \neq \frac{\alpha-1}{\tau-1} = 1.69$. **D)** The instantaneous size as a function of time is calculated for all avalanches, which are combined according to duration into five distinct groups. **E)** The shape of the profile is similar for all avalanches, as seen by replotting the data shown in D), with the timescale normalized by the duration, T , (*i.e.*,

$t \rightarrow t/T$) and after the size of each avalanche is scaled by a power-law of the duration (*i. e.*, $s \rightarrow s/T^\gamma$), in which $\gamma = \frac{1}{\sigma_{VZ}} - 1 = 0.80$. **F**) The scale-free behavior is seen more clearly by using a fitted value of γ , $\gamma^{opt} = 0.90$, obtained from the mean value of each curve. The code that generated this figure is available online as `avalanche_data.m`.

If the system is critical, then its activity should be scale-free, meaning the distribution of trajectories (number of spikes per time-bin versus time) of avalanches of different sizes can be multiplicatively scaled to appear identical (*cf.* Figure 7.16D-E). Such scale-free activity does not mean the system is a scale-free network, which means the connectivity pattern is scale-free—critical networks can have local connectivity. Scale-free activity in avalanches can be tested in two ways.

Box 7.20. Scale-free activity: Activity that cannot be ascribed a particular length-scale or time-scale over which correlations decay.

Box 7.21. Scale-free network: A network whose connections are not confined to or dominated by a particular length-scale.

Box 7.22. Universal curve: A curve onto which multiple datasets fall, if each dataset has its x-coordinate and y-coordinate scaled by separate appropriate values that are related to each other.

First, the mean instantaneous size of all avalanches of a given duration can be plotted as a function of time (Figure 7.16D). All avalanches begin with an increase of activity from zero and they finish when the activity returns to zero. If the activity is scale-free, the shape of the curve describing how the mean activity increases then falls back toward zero is independent of the total duration of the set of avalanches being averaged. That is to say a universal curve exists, so that if the curves produced from different durations are scaled appropriately, they will lie on top of each other if the system is critical and therefore scale-free.

To see whether avalanches produce a universal curve, the time index should be scaled by (*i. e.*, normalized by or divided by) the total duration of the avalanche. So, we recalculate time for each avalanche as the fraction of the avalanche's duration. The appropriate scaling of instantaneous size as a function of time can be calculated from the relationship between the total sizes of avalanches, $S(T)$, and their duration, T .

To see this, let us assume that the mean peak size of avalanches scales according to the duration of avalanches by a factor of T^γ , where $\gamma > 0$ (longer avalanches have greater peak instantaneous size). If the curve is universal then the mean size at any fraction of the duration of the avalanche also scales by T^γ . Now the total size of the avalanche is the sum of the instantaneous size across all time bins. Even if the instantaneous size did not change, longer avalanches would have greater total size by a factor of T (for example, if each avalanche comprises a series of time bins with one neuron/site active in each time bin then the total size of each avalanche would be the number of time bins, T .) Therefore, if the instantaneous size also increases, in this case by a factor of T^γ , the total size of the

avalanche across all time bins is proportional to $T^{\gamma+1}$. However, we have already found the exponent for the total mean size of avalanches, $\langle S \rangle(T) \propto T^{\frac{1}{\sigma v z}}$ so we can identify $\frac{1}{\sigma v z}$ as equal to $\gamma + 1$, or equivalently obtain γ as:

$$\gamma = \frac{1}{\sigma v z} - 1. \quad \text{Eq. 7.12}$$

This result is proven in the Appendix.

In Figure 7.16E, we replot Figure 7.16D, but after dividing all size values by $T^{\frac{1}{\sigma v z}-1}$ and after dividing all time values by T for each avalanche of duration T . As can be seen, the curves are similar, but with a systematic shift mainly because the total size does not scale exactly as a power law (in Figure 7.16C the curve is slightly supralinear).

A second, quicker test (but a less rigorous one) of scale-free behavior relies upon comparison of the three exponents calculated in Eq. 7.9-7.11. If avalanches are scale-free in the manner described in the previous paragraphs, then the exponents are not independent, but satisfy the equation:

$$\frac{\alpha - 1}{\tau - 1} = \frac{1}{\sigma v z}, \quad \text{Eq. 7.13}$$

which is known as the scaling relation. The result is derived in the Appendix. The breakdown of scaling observed in Figure 7.16E means that Eq. 7.13 does not quite hold for the exponents calculated for such a simplified, near-critical system.

7.9.3. A simplified avalanche model with a subset of the features of criticality

The data used to obtain the power-law curves in Figure 7.16 are obtained from the birth-death process described below (see the online code `avalanche_data.m`). Each avalanche is initiated with a single active unit. At each time-step thereafter that active unit becomes inactive (a ‘death’) but gives rise to a number of new active units. The number of new active units (‘births’) is probabilistically chosen from the Poisson distribution with a mean of exactly 1. The process is repeated on the next time step, with a random number of ‘births’ produced by each active unit so that the number of active units in the next time step is the sum of all these ‘births’. That is, the number of active units, N_{i+1} , in time step $i + 1$, depends on the number of active units, N_i , in time step i , as:

$$N_{i+1} = \sum_{n=1}^{N_i} B_n \quad \text{Eq. 7.14}$$

where each value, B_n , (the random number of newly activated units or ‘births’ produced by each previously active unit) is the realized value of a Poisson process. That is, each B_n can be any non-negative integer, chosen with probability $P(B_n)$ given by:

$$P(B_n) = \frac{e^{-1}}{B_n!}. \quad \text{Eq. 7.15}$$

If a time-bin, i , is reached, where all the randomly chosen values of B_n are zero, so that $N_{i+1} = 0$, then the duration of the avalanche is recorded as $T = i$ and the total size is recorded as $S = \sum_{i=1}^T N_i$.

The avalanches produced by this model do exhibit power-law (or nearly power-law) statistics (Figures 7.16A-C). Moreover, the mean shapes of the avalanches are approximately universal (Figure 7.16F), meaning the system is close to criticality. The

expected scaling relationships are not quite achieved, mainly because of deviations at the level of very small avalanches, where the discrete time bins and discrete numbers of active units limit scale-free behavior. Since the smallest avalanches are the most numerous, they can play a dominant role when fitting the exponents.

More generally, scale-free behavior is limited for small avalanches by the discrete counting of neurons, and for large avalanches by the finite number of neurons being recorded. Given these restrictions, observation of scale-free behavior in neural systems is rarely as clear as that depicted by data such as these, obtained from computer simulations (albeit time-consuming ones) of a simple model.

7.10. Tutorial 7.2. Diverse dynamical systems from similar circuit architectures.

Neuroscience goals: learn how near-identical circuits can produce very different types of activity; learn how highly simplified neural circuits can nevertheless produce complex patterns of activity.

Computational goals: more practice at using matrices and arrays to simulate coupled units; the idea of using a single code or function to simulate multiple types of circuit by changing particular parameters.

For each question you will simulate a two-unit or three-unit circuit (*i. e.*, $N_{units} = 2$ or 3),

with connection matrices defined as $\underline{W} = \begin{pmatrix} W_{11} & W_{12} \\ W_{21} & W_{22} \end{pmatrix}$ or $\underline{W} = \begin{pmatrix} W_{11} & W_{12} & W_{13} \\ W_{21} & W_{22} & W_{23} \\ W_{31} & W_{32} & W_{33} \end{pmatrix}$,

respectively, where W_{ij} is the connection strength from unit i to unit j . Each unit, i , responds to a total input current, I_i , which is given by:

$$I_i = I_i^{(app)} + \sum_{j=1}^{N_{units}} W_{ji} r_j,$$

where $I_i^{(app)}$ is an external, applied current. Each unit responds with a threshold-linear firing-rate curve, so that

$$\tau \frac{dr_i}{dt} = -r_i + I_i - \Theta_i,$$

with time constant, $\tau=10$ ms, and where Θ_i is the threshold for unit i . If the threshold is negative, it denotes the level of spontaneous activity in the unit in the absence of input current.

To ensure rates are positive and do not exceed a maximum, we include the further conditions: $0 \leq r_i \leq r_{max}$, where $r_{max} = 100$ Hz.

The values of connection strengths and thresholds will vary across the nine circuits you will simulate. For each circuit, determine what sort of dynamical system is produced. For example, find the number of distinct states within the circuit or whether the system is chaotic or possesses a heteroclinic sequence. You should use pulses of applied current or changes in the initial conditions to aid your analysis.

Try to write the code with only a single loop for the time simulation written in the code and a separate loop to run through the 9 questions with different parameters. You can use the commands `match` and `case` in Python to update the parameters for each question.

1) $\underline{W} = \begin{pmatrix} 0.6 & 1 \\ -0.2 & 0 \end{pmatrix}, \Theta_1 = -5, \Theta_2 = -10.$

2) $\underline{W} = \begin{pmatrix} 1.2 & -0.3 \\ -0.2 & 1.1 \end{pmatrix}, \Theta_1 = 10, \Theta_2 = 5.$

3) $\underline{W} = \begin{pmatrix} 2.5 & 2 \\ -3.0 & -2 \end{pmatrix}, \Theta_1 = -10, \Theta_2 = 0$

4) $\underline{W} = \begin{pmatrix} 0.8 & -0.2 \\ -0.4 & 0.6 \end{pmatrix}, \Theta_1 = -10, \Theta_2 = -10.$

5) $\underline{W} = \begin{pmatrix} 2 & 1 \\ -1.5 & 0 \end{pmatrix}, \Theta_1 = 0, \Theta_2 = 20.$

6) $\underline{W} = \begin{pmatrix} 1.5 & 0 & 1 \\ 0 & 2 & 1 \\ -2.5 & -3 & -1 \end{pmatrix}, \Theta_1 = -10, \Theta_2 = -5, \Theta_3 = 5.$

7) $\underline{W} = \begin{pmatrix} 2.2 & -0.5 & 0.9 \\ -0.7 & 2 & 1.2 \\ -1.6 & -1.2 & 0 \end{pmatrix}, \Theta_1 = -18, \Theta_2 = -15, \Theta_3 = 0.$

8) $\underline{W} = \begin{pmatrix} 2.05 & -0.2 & 1.2 \\ -0.05 & 2.1 & 0.5 \\ -1.6 & -4 & 0 \end{pmatrix}, \Theta_1 = -10, \Theta_2 = -20, \Theta_3 = 10.$

9) $\underline{W} = \begin{pmatrix} 0.98 & -0.015 & -0.01 \\ 0 & 0.99 & -0.02 \\ -0.02 & 0.005 & 1.01 \end{pmatrix}, \Theta_1 = -2, \Theta_2 = -1, \Theta_3 = -1.$

Questions for Chapter 7.

1) Which combination of changes in parameters—either increasing or decreasing the feedback connection strength, while either increasing or decreasing the threshold of a unit—can have the effect of enhancing the overall stability of a bistable unit with positive feedback?

2) Two nullclines cross at five different points. What is the greatest number of stable fixed points the corresponding system can possess?

3) In an inhibition-stabilized circuit, the inhibitory neurons gain some extra excitatory input to reach a new stable state. In what direction do the following change (if they change at all)?

- a) The firing-rate of inhibitory cells.
- b) The firing-rate of excitatory cells.
- c) The total inhibitory input to excitatory cells.

- d) The total excitatory input to excitatory cells.
- e) The total inhibitory input to inhibitory cells.
- f) The total excitatory input to inhibitory cells.

4) Suggest one way in which chaotic activity would be beneficial for the brain and one way in which it would be detrimental.

7.11. Appendix. Proof of the scaling relationship for avalanche sizes

1) Proof of Eq. 7.12, that $\frac{1}{\sigma_{VZ}} = \gamma + 1$.

If avalanches are scale-free, then the instantaneous mean size, $\langle s \rangle$, as a function of time, t , for avalanches of total duration, T , can be written as:

$$\langle s \rangle(t, T) = s_0 \left(\frac{t}{T} T_0, T_0 \right) \cdot \left(\frac{T}{T_0} \right)^\gamma \quad \text{Eq. 7.16}$$

where s_0 is the universal function, describing the mean shape of avalanches, where we set the “standard” avalanche to have a duration of T_0 . The change in variable of the instantaneous time t , into $\frac{t}{T} T_0$, is done so that when t is a given fraction of T for any example avalanche, the equivalent time on the standard avalanche should be the same fraction of T_0 , that is $t/T = (\frac{t}{T} T_0)/T_0$.

The mean total size of avalanches of length T is then found by integrating over all instantaneous sizes:

$$\begin{aligned} \langle S \rangle(T) &= \int_0^T \langle s \rangle(t, T) dt \\ &= \int_0^T s_0 \left(\frac{t}{T} T_0, T_0 \right) \cdot \left(\frac{T}{T_0} \right)^\gamma dt \\ &= \left(\frac{T}{T_0} \right)^\gamma \int_0^{T_0} s_0(t', T_0) dt' \left(\frac{T}{T_0} \right) \quad (\text{substituting } t' = \frac{t}{T} T_0, \text{ so } dt = dt' \left(\frac{T}{T_0} \right)) \\ &= \left(\frac{T}{T_0} \right)^{\gamma+1} \langle S \rangle(T_0). \end{aligned} \quad \text{Eq. 7.17}$$

Therefore, the total size of avalanches of duration T would scale as $T^{\gamma+1}$, so we can make the identity $\frac{1}{\sigma_{VZ}} = \gamma + 1$ (Eq. 7.12), since $\frac{1}{\sigma_{VZ}}$ is already defined in Eq. 7.11 as the exponent in the power-law relationship between mean total size and duration of avalanches.

2) Proof of Eq. 7.13, that $\frac{1}{\sigma_{VZ}} = \frac{\alpha-1}{\tau-1}$.

We will calculate the distribution of total sizes of avalanches, assuming three properties that are true for critical systems:

Property A. The distribution of avalanche durations is a power-law with exponent $-\alpha$;

Property B. The probability of an avalanche of a given size, if we know the duration, is scale-free (so only depends on the mean size of that duration);

Property C. The mean size of a given duration is also a power-law, with exponent $\frac{1}{\sigma_{VZ}}$.

We can begin by writing the relationship between distributions of total size, $P(S)$, and duration, $P(T)$, as:

$$P(S) = \int P(T) P(S|T) dT, \quad \text{Eq. 7.18}$$

where $P(S|T)$ is the probability of the total size being S when the duration is T .

The key step is to notice then that if the shape of the distribution of sizes as a function of duration is scale-free (Property B), with a mean size that increases with duration as $T^{\frac{1}{\sigma_{VZ}}}$ (Property C), then the spread of sizes of the distribution scales by the same

factor as its mean, $T^{\frac{1}{\sigma v z}}$. Given the area of the distribution must be fixed at 1 (it is a probability distribution, so the area is the total probability of an avalanche having some value of size) then its height scales down by the increase in width, which introduces a factor of $T^{-\frac{1}{\sigma v z}}$. We can then write:

$$P(S|T) = T^{-\frac{1}{\sigma v z}} f\left(\frac{S}{T^{\frac{1}{\sigma v z}}}\right), \quad \text{Eq. 7.19}$$

where f is an arbitrary function, which, we do not need to know to find the scaling relation (just as we do not need to know the shape of $P(S|T)$).

We now use $P(T) = AT^{-\alpha}$ (Property A) and substitute Eq. 7.19 into equation Eq. 7.18 to find

$$P(S) = \int AT^{-\alpha} T^{-\frac{1}{\sigma v z}} f\left(\frac{S}{T^{\frac{1}{\sigma v z}}}\right) dT. \quad \text{Eq. 7.20}$$

We are only concerned with how this result depends on size, S , so do not need to evaluate the integral exactly (which we can not do anyway, while the function f is undefined). We proceed by making the substitution $x = \frac{S}{T^{\frac{1}{\sigma v z}}} = ST^{-\frac{1}{\sigma v z}}$, so $T = S^{\sigma v z} x^{-\sigma v z}$ and $dT = -\sigma v z S^{\sigma v z} x^{-\sigma v z - 1}$, which leads to a rewriting of Eq. 7.20 as:

$$P(S) = A \sigma v z S^{\sigma v z} S^{-1} S^{-\alpha \cdot \sigma v z} \int f(x) dx. \quad \text{Eq. 7.21}$$

The term with the integral now produces a constant that is independent of S or T , which we do not need to know. The preceding terms show us that the probability distribution is a power-law in S , with an exponent of $\sigma v z - 1 - \alpha \cdot \sigma v z$. Comparing this form with $P(S) \propto S^{-\tau}$ allows us to equate the exponents, so that:

$$-\tau = \sigma v z - 1 - \alpha \cdot \sigma v z, \quad \text{Eq. 7.22}$$

which can be rearranged to show the relationship (Eq. 7.13) between the scaling exponents that we aimed to prove:

$$\frac{1}{\sigma v z} = \frac{\alpha - 1}{\tau - 1}. \quad \text{Eq. 7.23}$$

References for Chapter 7

1. Izhikevich EM. *Dynamical Systems in Neuroscience: The Geometry of Excitability and Bursting*. Cambridge, MA, USA; London, England: MIT Press; 2007.
2. Strogatz SH. *Nonlinear Dynamics and Chaos*. 2nd ed. Boulder, CO: Westview Press; 2015.
3. Shenoy KV, Sahani M, Churchland MM. Cortical control of arm movements: a dynamical systems perspective. *Annu Rev Neurosci*. 2013;36:337-359.
4. Nagumo J, Arimoto S, Yoshizawa S. An active pulse transmission lines simulating nerve axon. *Proc IRE*. 1962;50:2061-2070.
5. Fitzhugh R. Impulses and physiological states in models of nerve and membrane. *Biophysical Journal*. 1961;1:445-466.
6. Izhikevich EM, Fitzhugh R. FitzHugh-Nagumo model. *Scholarpedia*. 2006;1(9):1349.
7. Tsodyks MV, Skaggs WE, Sejnowski TJ, McNaughton BL. Paradoxical effects of external modulation of inhibitory interneurons. *J Neurosci*. 1997;17(11):4382-4388.
8. Ozeki H, Finn IM, Schaffer ES, Miller KD, Ferster D. Inhibitory stabilization of the cortical network underlies visual surround suppression. *Neuron*. 2009;62(4):578-592.
9. Rubin DB, Van Hooser SD, Miller KD. The stabilized supralinear network: a unifying circuit motif underlying multi-input integration in sensory cortex. *Neuron*. 2015;85(2):402-417.
10. Shadlen MN, Newsome WT. The variable discharge of cortical neurons: implications for connectivity, computation, and information coding. *The Journal of neuroscience : the official journal of the Society for Neuroscience*. 1998;18(10):3870-3896.
11. Miller P. Itinerancy between attractor states in neural systems. *Curr Opin Neurobiol*. 2016;40:14-22.
12. Rubin E. *Synsoplevede Figurer: Studier i psykologisk Analyse. Forste Del [Visually experienced figures: Studies in psychological analysis. Part one]*. Copenhagen and Christiania: Gyldendalske Boghandel, Nordisk Forlag, University of Copenhagen; 1915.
13. Levelt WJ. Note on the distribution of dominance times in binocular rivalry. *Br J Psychol*. 1967;58(1):143-145.
14. Brascamp JW, Klink PC, Levelt WJ. The 'laws' of binocular rivalry: 50 years of Levelt's propositions. *Vision Res*. 2015;109(Pt A):20-37.
15. Levelt WJM. On binocular rivalry1965, Soesterberg, The Netherlands.
16. Hupe JM, Rubin N. The dynamics of bi-stable alternation in ambiguous motion displays: a fresh look at plaids. *Vision Res*. 2003;43(5):531-548.
17. Hupe JM, Rubin N. The oblique plaid effect. *Vision Res*. 2004;44(5):489-500.
18. Pressnitzer D, Hupe JM. Temporal dynamics of auditory and visual bistability reveal common principles of perceptual organization. *Current biology : CB*. 2006;16(13):1351-1357.
19. Winkler I, Denham S, Mill R, Bohm TM, Bendixen A. Multistability in auditory stream segregation: a predictive coding view. *Philos Trans R Soc Lond B Biol Sci*. 2012;367(1591):1001-1012.
20. Moreno-Bote R, Rinzel J, Rubin N. Noise-induced alternations in an attractor network model of perceptual bistability. *J Neurophysiol*. 2007;98(3):1125-1139.

21. Shpiro A, Moreno-Bote R, Rubin N, Rinzel J. Balance between noise and adaptation in competition models of perceptual bistability. *J Comput Neurosci.* 2009;27(1):37-54.
22. Afraimovich VS, Zhigulin VP, Rabinovich MI. On the origin of reproducible sequential activity in neural circuits. *Chaos.* 2004;14(4):1123-1129.
23. Huerta R, Rabinovich M. Reproducible sequence generation in random neural ensembles. *Physical Review Letters.* 2004;93(23):238104.
24. Rabinovich MI, Huerta R, Varona P, Afraimovich VS. Generation and reshaping of sequences in neural systems. *Biol Cybern.* 2006;95(6):519-536.
25. Churchland MM, Yu BM, Cunningham JP, et al. Stimulus onset quenches neural variability: a widespread cortical phenomenon. *Nature Neuroscience.* 2010;13(3):369-378.
26. Rajan K, Abbott LF, Sompolinsky H. Stimulus-dependent suppression of chaos in recurrent neural networks. *Phys Rev E Stat Nonlin Soft Matter Phys.* 2010;82(1 Pt 1):011903.
27. Sussillo D, Abbott LF. Generating coherent patterns of activity from chaotic neural networks. *Neuron.* 2009;63(4):544-557.
28. Laje R, Buonomano DV. Robust timing and motor patterns by taming chaos in recurrent neural networks. *Nat Neurosci.* 2013;16(7):925-933.
29. Bertschinger N, Natschlager T. Real-time computation at the edge of chaos in recurrent neural networks. *Neural Comput.* 2004;16(7):1413-1436.
30. Rabinovich MI, Abarbanel HD. The role of chaos in neural systems. *Neuroscience.* 1998;87(1):5-14.
31. Nowak MA, Sigmund K. Evolutionary dynamics of biological games. *Science.* 2004;303(5659):793-799.
32. van Vreeswijk C, Sompolinsky H. Chaos in neuronal networks with balanced excitatory and inhibitory activity. *Science.* 1996;274(5293):1724-1726.
33. Sompolinsky H, Crisanti A, Sommers HJ. Chaos in random neural networks. *Phys Rev Lett.* 1988;61(3):259-262.
34. Bak P, Paczuski M. Complexity, contingency, and criticality. *Proc Natl Acad Sci U S A.* 1995;92(15):6689-6696.
35. Bak P, Tang C, Wiesenfeld K. Self-organized criticality: An explanation of the 1/f noise. *Phys Rev Lett.* 1987;59(4):381-384.
36. Tkacik G, Mora T, Marre O, et al. Thermodynamics and signatures of criticality in a network of neurons. *Proc Natl Acad Sci U S A.* 2015;112(37):11508-11513.
37. Beggs JM, Plenz D. Neuronal avalanches in neocortical circuits. *The Journal of neuroscience : the official journal of the Society for Neuroscience.* 2003;23(35):11167-11177.
38. Beggs JM. The criticality hypothesis: how local cortical networks might optimize information processing. *Philos Trans A Math Phys Eng Sci.* 2008;366(1864):329-343.
39. Beggs JM, Timme N. Being critical of criticality in the brain. *Front Physiol.* 2012;3:163.